Caspase-mediated cleavage of murine norovirus NS1/2 potentiates apoptosis and is required for persistent infection of intestinal epithelial cells

Bridget A. Robinson[1], Jacob A. Van Winkle[1], Broc T McCune[2], A. Mack Peters[1], and Timothy J. Nice[1]*

[1]Department of Molecular Microbiology and Immunology, Oregon Health and Science University, Portland, Oregon, USA

[2]Department of Microbiology, University of Texas Southwestern Medical Center, Dallas, TX, USA

*Correspondence: Timothy J. Nice, nice@ohsu.edu

Short title: Cleavage of MNV NS1/2 potentiates death and is required for persistence

Abstract

Human norovirus (HNoV) is the leading cause of acute gastroenteritis and is spread by fecal shedding that can often persist for weeks to months after the resolution of symptoms. Elimination of persistent viral reservoirs has the potential to prevent outbreaks. Similar to HNoV, murine norovirus (MNV) is spread by persistent shedding in the feces and provides a tractable model to study molecular mechanisms of enteric persistence. Previous studies have identified non-structural protein 1 (NS1) from the persistent MNV strain CR6 as critical for persistent infection in intestinal epithelial cells (IECs), but its mechanism of action remains unclear. We now find that the function of CR6 NS1 is regulated by apoptotic caspase cleavage. Following induction of apoptosis in infected cells, caspases cleave the precursor NS1/2 protein, and this cleavage is prevented by mutation of caspase target motifs. These mutations profoundly compromise CR6 infection of IECs and persistence in the intestine. Conversely, NS1/2 cleavage is not required for acute replication in extra-intestinal tissues or in cultured myeloid cells, indicating an IEC-specific role. Intriguingly, we find that caspase cleavage of NS1/2 reciprocally promotes caspase activity, potentiates cell death, and amplifies spread among cultured IEC monolayers. Together, these data indicate that the function of CR6 NS1 is regulated by apoptotic caspases, and suggest that apoptotic cell death enables epithelial spread and persistent shedding.

Author Summary

Human Norovirus infection is highly contagious and the most common cause of acute gastroenteritis. Norovirus can be persistently shed after resolution of symptoms, perpetuating or initiating new outbreaks. Murine norovirus (MNV) is also persistently shed, enabling study of host and viral determinants of norovirus pathogenesis. We previously identified a critical role for MNV non-structural protein 1 (NS1), in persistence. Herein we find that regulation of NS1 by host apoptotic caspases is required for infection of intestinal epithelial cells, but not for extra-intestinal spread. Additionally, we demonstrate that NS1 reciprocally promotes cell death and spread among epithelial cells. These data identify regulation of NS1 by host proteases and suggest that apoptotic death is a determinant of epithelial spread and persistence.

42 **Introduction**

43 Human norovirus (HNoV) is the most common cause of epidemic gastroenteritis worldwide,
44 and can be particularly dangerous for infants and the elderly [1,2]. Viral shedding often persists
45 asymptomatically for weeks to months after acute infection [3,4], and is a potential source for
46 initiation of outbreaks. Despite recent success in development of *in vitro* systems to study HNoV
47 infection [5,6], there remains a need for robust small animal models for investigating NoV biology.
48 Murine norovirus (MNV) shares genotypic (ssRNA, positive-sense, ~7.5kb genome) and
49 phenotypic (fecal-oral transmission, infection of intestinal epithelial cells (IECs), persistent
50 shedding) features with HNoV. Therefore, studies of MNV have enabled considerable advances
51 in understanding of norovirus biology [7–9].

52 All noroviruses express a non-structural polyprotein encoded by ORF1 and two structural
53 capsid proteins (VP1 and VP2) encoded by ORFs 2 and 3, respectively [10–12] (Fig. 1A). The
54 non-structural polyprotein is cleaved by the internally-encoded viral protease into six 'mature'
55 proteins (NS1/2, NS3, NS4, NS5, NS6, and NS7) [12–14]. Unlike related caliciviruses, NS1/2 of
56 NoV remains intact for most of the virus life cycle and may be cleaved by host proteases rather
57 than the viral protease [12,13]. NoV non-structural proteins associate with membranes and form
58 the membranous viral replication complex [15–18]. Specific roles of NS5-7 have been defined as
59 VpG cap, protease, and polymerase, respectively. However, the roles of NS1-4 are less well
60 understood [19].

61 Our prior MNV studies compared acute strain CW3 and persistent strain CR6 to identify
62 viral determinants of pathogenesis and persistence [20–22]. We found that the capsid gene of
63 CW3 ($VP1^{CW3}$) promotes extra-intestinal spread, whereas the NS1 gene of CR6 ($NS1^{CR6}$)
64 promotes intestinal replication and persistent fecal shedding. Persistent and non-persistent
65 strains similarly infect macrophages, dendritic cells, T-cells, and B-cells *in vitro* and *in vivo*
66 [6,23,24], and utilize the same cell-surface receptor, CD300lf [25,26]. However, recent studies

67 have shown that tropism for IECs *in vivo* requires NS1^{CR6} in addition to CD300lf expression by
68 non-hematopoietic cells [27,28]. Furthermore, only a minor lineage of IECs called tuft cells
69 naturally express CD300lf and are susceptible to persistent infection by CR6 [27,29]. In contrast
70 to the strain-dependent infection of IECs *in vivo*, CW3 and CR6 can replicate to similar titer in a
71 cultured IEC cell line (M2C) that ectopically expresses CD300lf [28]. Thus, NS1^{CR6} promotes IEC
72 persistence *in vivo* via mechanisms other than receptor usage or replicative capacity *per se*.

73 In addition to viral determinants of MNV infection, critical aspects of the host anti-viral
74 response have been identified. In particular, innate control of MNV replication is determined by
75 the compartmentalized roles of type I (α/β) and type III (λ) interferon (IFN) [30]. Both types of IFN
76 stimulate antiviral gene expression, but the IFN-α/β receptor (IFNAR) is expressed on most cell
77 types, whereas the IFN-λ receptor (IFNLR) is preferentially expressed on epithelial cells [30].
78 Correspondingly, IFN-α/β is critical for control of MNV in myeloid cells and prevents pathological
79 dissemination [23,31,32], whereas IFN-λ is critical for control of MNV in IECs and prevents
80 persistent shedding [33,34]. Deficiency of IFNLR promotes persistent infection, suggesting that
81 NS1^{CR6} counteracts the IFN-λ response [28]. However, CW3 persistence is not rescued in IFNLR-
82 deficient mice [28,34] indicating that other host pathways are also important.

83 In addition to the IFN response, a general host response to many diverse viral genera is
84 initiation of apoptosis. Correspondingly, viruses have evolved ways to hijack apoptotic machinery
85 to their benefit. Apoptosis is a non-inflammatory, highly-regulated disassembly of the cell
86 mediated by a family of cysteine proteases (caspases). Apoptotic cellular contents are packaged
87 and released in membranous apoptotic bodies to be taken up by professional phagocytes and
88 other neighboring cells [35]. Because apoptosis is an innate response to infection, many viruses
89 have developed ways to delay induction of apoptosis such as expression of anti-apoptotic Bcl-2
90 family homologues [36,37]. In contrast, after virus production has reached its peak, many viruses
91 actively promote apoptotic death or utilize 'apoptotic mimicry' to facilitate viral dissemination

92 [37,38]. Additionally, some viruses rely on apoptotic caspases to cleave viral proteins as an
93 additional level of regulation [39–41]. Thus, depending on its timing in relation to viral replication,
94 apoptosis can be anti-viral or pro-viral and is therefore regulated by a diverse array of viral
95 mechanisms.

96 HNoV and MNV infection both induce apoptosis, as indicated by association with markers
97 of apoptosis in infected intestinal tissue [42–44]. Thus, these viruses have likely also developed
98 mechanisms to regulate apoptosis in a pro-viral manner. Apoptosis has been most extensively
99 studied in MNV-infected myeloid cells and is associated with down-regulation of anti-apoptotic
100 survivin protein and activation of caspases 3, 7, and 9 [45,46]. Expression of the MNV ORF1
101 polyprotein is sufficient to induce apoptosis [47], indicating that one or more non-structural
102 proteins are pro-apoptotic in the absence of viral replication. Additionally, NS1/2 encodes caspase
103 cleavage motifs that are targeted by recombinant caspase 3 in a cell-free assay and separate
104 NS1 from membrane-associated NS2 [12]. Thus, apoptosis during MNV infection may be
105 facilitated by non-structural proteins and host caspases may reciprocally regulate NS1/2 function
106 [20].

107 Herein, we identify a critical role for NS1/2 cleavage during MNV infection and intestinal
108 persistence. We demonstrate that at late times post-infection, concurrent with induction of
109 apoptosis, a minority of total NS1/2 protein is cleaved in a caspase-dependent manner. Despite
110 the relatively low proportion of total NS1/2 that is cleaved, NS1/2^{CR6} cleavage is absolutely
111 required for persistent infection in IECs, independent of IFN-λ. Moreover, the cleavage of
112 NS1/2^{CR6} promotes apoptotic death of infected myeloid cells and spread among cultured IECs.
113 These data suggest that controlled induction of apoptosis during viral egress promotes spread
114 among IECs and is required for maintenance of the persistent cellular reservoir.

115 **Results**

116 **Host caspases cleave NS1/2 at late times post-infection**. Previous cell-free studies identified
117 two functional caspase motifs (DKAD^{121} and DAMD^{131}) within NS1/2 that are cleaved by host
118 caspase 3 [12] (Fig. 1A), however, the targeting of these sites during infection and functional
119 consequences of NS1/2 cleavage was unknown. To test their role in persistent infection, we
120 mutated these sites (D121G and D131G) within MNV strain, CR6 (CR6$^{\Delta casp}$, Fig. 1B). In parallel,
121 we generated a variant of CR6$^{\Delta casp}$ with the capsid of the systemic strain CW3 (CR6$^{\Delta casp}$-VP1^{CW3})
122 to enable determination of a role for NS1/2 cleavage in extra-intestinal tissues (Fig. 1B) [20,48].
123 Analysis of NS1/2 protein expression following infection of BV2 myeloid cells revealed a similar
124 level of full length NS1/2 production for all strains. However, infection with CW3, CR6, or the CR6-
125 VP1^{CW3} chimera but not NS1/2 cleavage mutant strains resulted in a ~28 kDa NS2 fragment
126 detectable at 18-22 hours post-infection (Fig. 1C). The ~18kDa NS1 protein was inconsistently
127 detected in cell lysate for any strain and may reflect the loss of dying cells or the small overall
128 proportion of cleaved NS1/2. Several fragments larger than 28 kDa (marked by *) were also
129 observed but did not consistently differ between strains, indicating they are independent of NS1/2
130 mutations (Fig. 1C). Overall, these data show that cleavage of NS1/2 occurs during infection,
131 depends on caspase motifs, and is independent of other genetic variation between CW3 and CR6.

132 To determine the temporal relationship between caspase activity and NS1/2 cleavage, we
133 detected cleaved caspase 3 (active form) by western blot. Cleaved caspase 3 was observed at
134 18-22 hours post-infection for all strains tested, concurrent with NS1/2 cleavage (Fig. 1D). To test
135 the requirement of caspase activity for NS1/2 cleavage, we treated infected cells with the pan-
136 caspase inhibitor, ZVAD-fmk. Inhibitor treatment reduced the proportion of cleaved caspase 3 and
137 NS2 in cells infected with CW3 or CR6 but did not reduce the abundance of NS1/2 fragments
138 larger than 28 kDa (Fig. 1D). Together, these data demonstrate that NS1/2 is cleaved 18-22 hours

139 post infection with persistent or non-persistent MNV strains, concurrent with induction of
140 apoptosis, in a caspase-dependent manner.
141
142 **NS1/2 cleavage promotes apoptosis in myeloid cells.** In the course of characterizing caspase
143 cleavage, we observed that the timing and magnitude of caspase 3 cleavage differed between
144 viral strains (Fig. 1D). To further compare caspase activity triggered by MNV infection, we used
145 densitometry to quantify percentage of cleaved caspase 3 and poly ADP-ribose polymerase
146 (PARP), a known target of apoptotic caspases [49]. We observed three-fold more activated
147 caspase 3 and 10-20% more cleaved PARP in cells 18 hours post-infection with CR6 compared
148 to CR6$^{\Delta casp}$ or CW3 (Fig. 2A-C). There were no significant differences in MNV polymerase (NS7)
149 detected for any infection condition suggesting that the difference in caspase 3 and PARP
150 cleavage was not simply due to increased replication in CR6-infected cultures (Fig. 2B). Together,
151 these data suggest that cleavage of CR6 NS1/2 (but not CW3 NS1/2) potentiates caspase activity.
152 To test whether our panel of MNV strains differed in induction of apoptotic cell death, we
153 quantified surface presentation of phosphatidylserine (PS, Annexin V staining) and permeability
154 to the LIVE/DEAD viability dye by flow cytometry following infection of BV2 cells (Fig. 1B). We
155 found that CR6 infection resulted in two-fold more apoptotic cells (Annexin V positive, LIVE/DEAD
156 negative) than CW3 or CR6$^{\Delta casp}$ (Fig. 2A-B). In contrast to CR6, most CR6-VP1^{CW3} infected cells
157 lost membrane integrity and were stained with the LIVE/DEAD dye (Fig. 2A-C), which is consistent
158 with our recent findings that VP1^{CW3} drives lytic cell death and inflammatory cytokine production
159 [48]. Even so, cells infected with CR6-VP1^{CW3} had 30-50% more total Annexin V staining than
160 cells infected with the corresponding mutant strain CR6$^{\Delta casp}$-VP1^{CW3}, indicating that NS1/2
161 cleavage promotes cell death in conjunction with VP1^{CW3}-dependent lysis (Fig. 2C). Together,
162 these data suggest that CR6 NS1/2 cleavage by apoptotic caspases reciprocally promotes
163 cleavage of caspase substrates and consequential cell death.

164

165 **Cleavage of NS1/2 is not required for *in vitro* MNV replication in myeloid cells.** The
166 abundance of full-length NS1/2 and NS7 on western blots was similar between WT and mutant
167 strains, indicating that viral protein production was unaffected by NS1/2 cleavage mutations (Fig.
168 1C-D, 2A). However, many additional steps beyond protein production are required for assembly
169 of infectious virus. So, we compared production of plaque forming units (PFU) over time from
170 myeloid cells infected with our panel of MNV strains (Fig. 1B) to assess whether production of
171 infectious virus was dependent on CR6 NS1/2 cleavage. Mutation of NS1/2 cleavage sites did not
172 significantly alter MNV replication kinetics or peak titers in BV2 cells following infection at a high
173 multiplicity of infection (MOI, one PFU/cell) (Fig. 3A). Following infection of BV2 cells at a low MOI
174 (0.01 PFU/cell), there were modest differences in early 10-18 hour titer, but all strains reached
175 similar peak titers by 36 hours post-infection (Fig. 3A). The similar peak titers are consistent with
176 our ability to obtain high titer viral stocks of NS1/2 cleavage mutants (generated by low MOI
177 infection of BV2 cells) and indicate that NS1/2 cleavage is not required for MNV replication in
178 these cells.

179 To test the requirement of NS1/2 cleavage for replication in primary myeloid cells, we
180 generated bone-marrow dendritic cells (BMDCs) and infected them with our panel of MNV strains.
181 Similar to BV2 cells, BMDC replication was minimally impacted by mutation of NS1/2 cleavage
182 sites (Fig. 3B-C). However, CW3 and CR6-VP1^{CW3} reached higher peak titer in WT BMDCs
183 compared to other strains tested, suggesting a VP1-dependent role in BMDC replication. In
184 parallel, we tested the role of STAT1-dependent IFN responses by comparing growth of our MNV
185 strains in *Stat1*$^{-/-}$ BMDCs. All MNV strains reached higher peak titers in *Stat1*$^{-/-}$ BMDCs compared
186 to WT BMDCs (compare Fig. 3B and 3C), as expected from prior studies of STAT1-dependent
187 immunity to MNV [23]. However, there were no statistically significant differences in growth that

188 could be attributed to NS1/2 cleavage (Fig.3C). Overall, these data indicate that NS1/2 cleavage
189 is not required for replication of MNV in myeloid cells.
190
191 **NS1/2 cleavage is not required for lethal systemic infection.** *Stat1*$^{-/-}$ mice succumb to infection
192 in a VP1^{CW3}-dependent manner due to a profound inability to control systemic replication in
193 myeloid cells [20–22,31,32]. To test whether NS1/2 cleavage mutations impair this pathological
194 MNV replication, we orally inoculated *Stat1*$^{-/-}$ mice with CR6-VP1^{CW3} or CR6$^{\Delta casp}$-VP1^{CW3} and
195 monitored animals daily for signs of distress. Infection with CW3 or CR6-VP1^{CW3} resulted in 100%
196 lethality with similar kinetics (Fig. 4A). As expected, CR6-infected controls remained healthy due
197 to lack of VP1^{CW3}-facilitated systemic spread [20]. These *in vivo* pathogenesis data suggest that
198 NS1/2 cleavage is not required for lethal pathology resulting from uncontrolled, systemic infection
199 of myeloid cells, consistent with no NS1/2 cleavage requirement for *in vitro* replication in myeloid
200 cells.
201
202 **NS1/2 cleavage is required for intestinal tropism and persistence**. To directly quantify the
203 effect of NS1/2 cleavage on acute replication and tissue tropism, we inoculated WT mice with
204 CR6, CR6$^{\Delta casp}$, CR6-VP1^{CW3}, or CR6$^{\Delta casp}$-VP1^{CW3} and analyzed tissue and stool titers at three
205 days post-infection (Fig. 4B). As expected from our prior studies, CR6 and CR6-VP1^{CW3} were
206 detected on day three in the mesenteric lymph node (MLN), ileum, and colon. We also detected
207 infectious virus shed in the feces of mice infected with CR6 and CR6-VP1^{CW3}, consistent with
208 replication in intestinal tissue. In contrast, in mice infected with NS1/2 cleavage mutant strains
209 CR6$^{\Delta casp}$ or CR6$^{\Delta casp}$-VP1^{CW3}, infectious virus was rarely detected in intestinal tissues, or being
210 shed in the feces. However, despite severely compromised replication in ileum (10-fold) and colon
211 (1000-fold), splenic titers of CR6$^{\Delta casp}$-VP1^{CW3} were not significantly different from CR6-VP1^{CW3}
212 (Fig. 4B). This indicates that NS1/2 cleavage is not required for systemic spread, consistent with

213 *Stat1*$^{-/-}$ lethality data (Fig. 4A). Overall, these acute titer data demonstrate that caspase cleavage
214 of NS1/2 is specifically required for promoting early infection of intestinal tissue, the eventual site
215 of persistence.

216 Due to limited early detection of NS1/2 cleavage mutants in the intestinal tissues, we
217 predicted that NS1/2 cleavage would be required for intestinal persistence. Indeed, most mice
218 infected with CR6$^{\Delta casp}$ or CR6$^{\Delta casp}$-VP1^{CW3} had undetectable viral genomes in tissues at 21 days
219 post-infection whereas CR6 and CR6-VP1^{CW3} were present in the ileum, colon, and stool (Fig.
220 4C). Altogether, these findings support a role for NS1/2 cleavage in establishing early infection of
221 the intestine and subsequent persistence.

222

223 **NS1/2 cleavage is required for intestinal persistence independent of IFN-λ.** IFN-λ plays a
224 critical role in protection against persistent MNV infection of the intestine [34], so we sought to
225 determine whether CR6$^{\Delta casp}$ persistence was restored in the absence of IFN-λ signaling. We
226 infected WT or *Ifnlr1*$^{-/-}$ mice with CR6 or CR6$^{\Delta casp}$ and monitored shedding in the stool over time
227 (Fig. 5A, B), and persistence in the colon at 21 days post-infection (Fig. 5C, D). Additionally, to
228 determine whether an early barrier to MNV infection could be overcome with increased infectious
229 dose, we included an experimental group inoculated with a 10-fold higher dose of CR6$^{\Delta casp}$ (1e7
230 PFU). MNV was shed in the stool of all WT mice infected with CR6 beginning on day three and
231 continuing until the experimental endpoint, day 21. Consistent with the known role of IFN-λ , *Ifnlr1*$^{-}$
232 $^{/-}$ mice infected with CR6 shed greater than 10-fold more virus relative to WT mice (Fig. 5A, B),
233 and CR6 was detected in colon tissue at levels commensurate with fecal shedding (Fig. 5C, D).
234 In contrast, we were unable to detect shedding or colonic persistence of CR6$^{\Delta casp}$ at any time from
235 WT or *Ifnlr1*$^{-/-}$ mice (Fig. 5A, B). These data indicate that CR6 NS1/2 cleavage promotes persistent
236 infection via a novel mechanism separate from IFN antagonism.

237

238 **Cleavage of NS1/2 is critical for MNV infection of intestinal epithelial cells.** Our preceding
239 data demonstrated that disrupting NS1/2 cleavage prevents intestinal infection and persistence in
240 either WT or *Ifnlr1*$^{-/-}$ mice (Fig. 4-5). Because intestinal persistence requires establishment of an
241 infected IEC reservoir, we hypothesized that NS1/2 cleavage promoted early IEC tropism. To test
242 this hypothesis, we infected WT or *Ifnlr1*$^{-/-}$ mice with our panel of MNV strains (Fig. 1B) and
243 quantified IEC infection at three days post-infection by flow cytometry. We pooled IECs isolated
244 from proximal colon, cecum, and distal small intestine (devoid of Peyer's patches), and stained
245 intracellularly for MNV NS1/2 (Fig. 6A-C). We rarely detected infected IECs in WT mice at this
246 early timepoint, indicating that acute infection of IECs in our WT mice is below the limit of detection
247 for this assay (Fig. 6B). However, IEC infection was increased in *Ifnlr1*$^{-/-}$ mice relative to WT mice,
248 indicating that IFN-λ limits early establishment of infection in the IEC reservoir (Fig. 6A, C). CR6
249 and CR6-VP1^{CW3} were detected in an average of 40 IECs per million in *Ifnlr1*$^{-/-}$ mice, but we did
250 not detect significant infection of IECs by NS1/2 cleavage mutants (Fig. 6C). To contextualize IEC
251 data, we quantified MNV infection of non-epithelial cells in Peyer's patches by qPCR. We detected
252 viral RNA in Peyer's patches for the majority of CR6-infected mice, ~50% of CR6$^{\Delta casp}$-infected
253 mice, and all mice infected with CR6-VP1^{CW3} or CR6$^{\Delta casp}$-VP1^{CW3} (Fig. 6D, E). These data suggest
254 that NS1/2 cleavage is not strictly required for initial infection of non-epithelial cells during acute
255 infection, particularly for the CR6-VP1^{CW3} strain that robustly infects Peyer's patches and spleen
256 (Figs 4B, 6C, D). Furthermore, the relationship between replication of MNV strains in Peyer's
257 patches of *Ifnlr1*$^{-/-}$ mice was similar to WT mice (Fig. 6C, D), consistent with a minimal role of IFN-
258 λ in non-epithelial cells. Together, these data indicate that NS1/2 cleavage promotes early
259 infection of IECs, independent of early replication in Peyer's patches.

260 In complementary experiments, we infected mice with our panel of MNV strains and
261 detected MNV genomes and EpCAM transcripts in small intestine sections via RNAscope at 48-
262 72 hours post-infection (Fig. 7). We included groups of WT and *Ifnar1 x Ifnlr1* double knockout

263 (DKO) mice to compare IFN-restricted and unrestricted tropism, respectively. We reproducibly
264 detected CR6 infection of IECs in WT mice at an average of 1 double positive (MNV and EpCAM)
265 cell per cm of tissue length, whereas CR6-VP1^{CW3} was not consistently detected in IECs of WT
266 mice and NS1/2 cleavage mutants were not detected at all (Fig. 7A-B). In DKO mice, CR6 and
267 CR6-VP1^{CW3} were detected with increased frequency relative to WT mice at seven and one DP
268 cells per cm tissue length, respectively (Fig. 7C-D). In contrast, infection of IECs by NS1/2
269 cleavage mutants remained below the limit of detection in DKO mice (Fig. 7E). Infection of non-
270 epithelial cells was observed inconsistently for all strains in WT mice and did not correlate with
271 IEC infection; in DKO mice, CR6-VP1^{CW3} and CR6$^{\Delta casp}$-VP1^{CW3} robustly infected non-epithelial
272 cells, whereas CR6 infection of non-epithelial cells remained inconsistent (Fig. 7F). Taken
273 together, these data demonstrate an IFN-independent role of NS1/2 cleavage in promoting early
274 infection of IECs, the cellular reservoir of MNV persistence.
275
276 **NS1/2 cleavage promotes spread among IEC monolayers.** The infected IECs we observed *in*
277 *vivo* on day three may be a result of viral amplification and spread rather than initial infection. To
278 directly test the role of NS1/2 cleavage on initial infection of IECs, we used a previously
279 characterized CD300lf-transduced IEC cell line (M2C-CD300lf, hereafter M2C), which can be
280 infected by CW3 and CR6 [28]. We infected M2C cells with our panel of persistent and non-
281 persistent strains (Fig. 1B) and quantified replication over time by plaque assay (Fig. 8A).
282 Following infection at an MOI of one, persistent strains (CR6 and CR6-VP1^{CW3}) produced
283 significantly more infectious progeny at 10 hours post-infection compared to non-persistent strains
284 (CW3, CR6$^{\Delta casp}$, or CR6$^{\Delta casp}$-VP1^{CW3}). However, between 18-48 hours post-infection all strains
285 reached similar peak titers with at most a two-fold difference between persistent and non-
286 persistent strains (Fig. 8A). Likewise, infection of M2C cells at a low MOI (0.01 PFU/cell) resulted
287 in higher titers for persistent strains at 10 hours post-infection, but all strains reached similar titers

288 by 18 hours post-infection (Fig. 8B). However, between 24-72 hours following low-MOI infection,
289 persistent strains proceeded to replicate robustly and reach similar peak titer as high MOI
290 infection, whereas non-persistent strains replicated more slowly with 10-fold lower titer between
291 24-72 hours (Fig. 8B). These findings differ from our earlier analysis in myeloid cells, where higher
292 peak titers did not correlate with persistence phenotype (Fig. 3), and suggest specific roles of CR6
293 NS1/2 cleavage in IEC infection.

294 To further characterize infection in IECs, we quantified infected cells by
295 immunofluorescence staining for MNV NS7 following infection at MOI of one. Unexpectedly, only
296 10% of M2C cells were NS7-positive at 14 and 24 hours post-infection, suggesting that MNV does
297 not efficiently initiate replication in these cells. However, strains CW3, CR6, or CR6$^{\Delta casp}$ all had a
298 similarly low percentage of initially infected cells (Fig. 8C, D). This equal infection suggests that
299 early differences in titer at 10 hours are due to different rates of virus production per cell. Although
300 the initial proportion of infected cells was similar between strains, the percentage of CR6-infected
301 cells increased from 10 to 30% by 32 hours whereas the percentage of CW3 or CR6$^{\Delta casp}$ infected
302 cells did not significantly increase (Fig. 8C, D). Furthermore, visual inspection of CR6-infected
303 M2C cell monolayers at 48-72 hours post-infection revealed patches of minimal cellularity
304 whereas CW3 or CR6$^{\Delta casp}$ infected monolayers remained intact (Fig. 8E). In sum, these data
305 indicate that non-persistent strains are similarly able to initially infect IECs, but spread among IEC
306 monolayers is facilitated by cleavage of CR6 NS1/2.

307

308 **NS1/2 cleavage promotes death of IECs.** We next sought to identify the cellular response
309 altered by NS1/2 cleavage that may account for differential spread among IEC monolayers and
310 establishment of IEC infection *in vivo*. Analyses in myeloid cells indicated that NS1/2 cleavage
311 promoted apoptotic cell death (Fig. 2). To test whether IEC apoptosis was also promoted by NS1/2
312 cleavage, we infected M2C monolayers with CW3, CR6, or CR6$^{\Delta casp}$ and characterized cleavage

313 of NS1/2, caspase 3, and PARP by western blot. In contrast to the robust caspase 3 cleavage
314 seen in infected BV2 cells, we detected less than 10% cleavage of caspase 3 in M2C lysates from
315 infection with any strain at any timepoint and were infrequently able to detect NS1/2 cleavage at
316 any time post-infection (Fig. 9A). This reduced cleavage is consistent with the relatively low
317 frequency of infected M2C cells and loss of cellularity in CR6-infected cultures (Fig. 8C-E).
318 Additionally, staurosporine treatment of M2C resulted in visible loss of cellularity, but less
319 cleavage of caspase 3 (25% vs. 60%) and PARP (10% vs. 95%) compared to BV2 cells (Fig. 9A-
320 E, 2A-E). Despite the relatively low amount of caspase cleavage, M2C monolayers infected with
321 CR6 had three-fold more caspase 3 and PARP cleavage than those infected with CW3 or CR6$^{\Delta casp}$
322 (Fig. 9A-C) with no significant difference in viral protein production (NS7, Fig. 9A, B). To determine
323 if differences in caspase activity of infected M2C cells correlated with a different proportion of
324 apoptotic cells, we quantified Annexin V staining and cell lysis by flow cytometry. No apoptotic
325 cells were detected in the first 24 hours post-infection (not shown), consistent with slower
326 replication kinetics and caspase activation (Fig. 8, 9A-C). However, by 36 hours post-infection
327 CR6 triggered a three-fold increase in apoptotic cells (Annexin V positive, LIVE/DEAD negative)
328 whereas CW3 or CR6$^{\Delta casp}$ triggered only a two-fold increase over background (Fig. 9D, E).
329 Altogether, these data demonstrate that CR6 NS1/2 cleavage promotes apoptotic caspase activity
330 and cell death of myeloid (BV2) and IEC (M2C) cell lines.

331 MNV-induced death occurred in a relatively low proportion of M2C cells over an extended
332 time course with strain-dependent loss of cellularity (Fig. 8E). To more comprehensively compare
333 strain-dependent differences in this context, we used the incucyte imaging system to quantify
334 confluency, Annexin V staining, and cytotox viability dye staining over time. Control M2C
335 monolayers treated with staurosporine died rapidly with loss of confluency and increasing Annexin
336 V and cytotox staining between 4-12 hours post-treatment (Fig. 10). CR6 infected monolayers
337 also lost confluency over the course of the experiment whereas CW3 or CR6$^{\Delta casp}$ infected

338 monolayers remained intact (Fig. 10A). Monolayers infected with all MNV strains became positive
339 for Annexin V and cytotox with similar kinetics, beginning at 24 hours post-infection and increased
340 to a maximum at 48 hours (Fig. 9A, B, S1-S5). However, CR6 infection resulted in more overall
341 Annexin V and cytotox staining over the course of the experiment than CW3 or CR6$^{\Delta casp}$ infection,
342 as quantified by area-under-curve (AUC) analyses (Fig. 9C). Although flow cytometry experiments
343 detected Annexin V positive M2C cells with intact membranes (Fig. 9D, E), these live imaging
344 data suggest that there is a rapid progression from apoptosis to lytic death in virally infected cells.
345 Overall, these analyses of cell death suggest that CR6 NS1/2 cleavage promotes increased
346 apoptotic and lytic death in IECs. Taken together with our *in vivo* data, we propose that NS1/2 is
347 a viral sensor of caspase activity whose cleavage promotes execution of cell death programs
348 during viral egress, lateral spread among intestinal epithelial cells, and persistent shedding (Fig.
349 11).
350

351 **Discussion**

352 Herein, we demonstrate that caspase-mediated cleavage of the nonstructural protein,
353 NS1/2, is critical for persistent MNV infection of the intestine. We engineered and characterized
354 a strain of MNV in which NS1/2 is not cleaved (CR6$^{\Delta casp}$), and our *in vitro* and *in vivo* analyses
355 demonstrate that NS1/2 cleavage is not required for viral replication in myeloid cells but is
356 specifically required for promoting infection in IECs, the cellular reservoir of persistence.
357 Furthermore, our data indicate that NS1/2 cleavage potentiates apoptosis and lytic death,
358 suggesting that regulation of cell death is a critical aspect of establishing a persistent MNV
359 infection in IECs.

360 NS1/2 was not previously known to play a role in cell death during MNV infection, but is
361 required for viral replication beginning at the earliest stages of replication complex assembly.
362 Norovirus replication occurs in the cytoplasm on cellular membranes with a variety of organelle
363 markers [15], and occurs near membranous vesicles [15,23]. MNV NS1/2 localizes to the
364 endoplasmic reticulum (ER) [16,17] and promotes replication via membrane re-organization and
365 through an interaction with the vesicle-associated membrane protein, VAPA [18,50]. Similarly,
366 HNoV NS1/2 interacts with VAPA, localizes to vesicles, and disrupts vesicle trafficking when
367 ectopically expressed [18]. Our data indicate that this early and essential role of NS1/2 remains
368 intact when the caspase cleavage sites are mutated, and viral replication occurs normally in
369 myeloid cells (Fig. 2). NS1/2 cleavage only occurs after viral replication has peaked indicating that
370 its role in promoting death, IEC infection, and persistence involves relatively late events in the
371 viral life cycle.

372 The last step of the MNV replication cycle is egress, which occurs concurrently with
373 induction of apoptosis. Therefore, NS1/2 cleavage and associated apoptotic death may be
374 important for regulating release of viral progeny. How noroviruses are released from infected cells
375 is not well understood, but infection of macrophages, DCs, or IECs does result in cell lysis ([23],

376 Figs. 2, 9, 10) and non-enveloped viruses generally rely on cell lysis to release newly assembled
377 virions. Apoptotic processes may alter egress by reducing lytic virion release and favoring
378 retention of virions within cellular membranes. Indeed, a number of non-enveloped viruses utilize
379 vesicle-associated egress as a means of evasion from immune detection, and vesicles with
380 exposed phosphatidylserine allow for phagocytic uptake of novel target cells that may not express
381 the viral receptor [51,52]. In addition to facilitating phagocytic uptake, membranes with PS can
382 inhibit IFN responses via activation of Tyro3/Axl/Mer (TAM) receptor tyrosine kinases on target
383 cells [53], which would allow more efficient viral replication. Thus, vesicular egress has the
384 potential to dramatically change the outcome of infection via biophysical and immunological
385 mechanisms. Intriguingly, recent studies by the Altan-Bonet group indicate that MNV can be
386 released from intact cells in PS-positive membranes [54] but the proportion of total virions
387 released in this manner remains unknown. Therefore, it will be important in future work to consider
388 the role of NS1/2 cleavage on regulation of this newly-described membranous egress and the role
389 of viral association with membranes on spread among IECs.

390 The MNV receptor CD300lf is specifically expressed on MNV target cells, including myeloid
391 cells and a specialized IEC subtype, tuft cells [25]. Tuft cells are a rare cell type in the intestinal
392 epithelium and are dispersed among non-tuft, CD300lf-negative IECs [55]. Our analyses often
393 found intestinal villi with multiple, adjacent epithelial cells infected (Fig. 7C), raising the possibility
394 of direct MNV spread to neighboring IECs, which could be mediated by cell death or apoptotic
395 egress and regulated by NS1/2 cleavage. Our *in vitro* studies of infection in IEC monolayers
396 support this hypothesis, and the dispersed nature of CD300lf-expressing tuft cells poses a strong
397 selective pressure for efficient spread across receptor-negative stretches of the intestinal
398 epithelium (Fig. 11). Recent development of *in vitro* methods for differentiating tuft cells in primary
399 IEC cultures [56] will enable future experiments to characterize spread in an IEC monolayer more
400 representative of the *in vivo* scenario.

401 Regular turnover of the intestinal epithelium results in a short lifespan for differentiated
402 epithelial cells, which undergo a specialized form of apoptotic cell death (anoikis) triggered as the
403 cell detaches from the basal membrane and is shed into the lumen [57]. Specific Bcl-2 family
404 proteins are critical players in anoikis [58,59], and display increased expression as IECs transit
405 up the villus [59]. It is possible cleavage of NS1/2 (and perhaps NS1 directly) interferes with Bcl-
406 2 family proteins as a means of altering the kinetics of the highly-regulated pathways that control
407 apoptosis within differentiated IECs. Interestingly, similar to NS1/2 cleavage promoting apoptosis
408 during infection, some Bcl-2 proteins (e.g. Bid) are also regulated via cleavage, in which the
409 truncated version is the active, pro-apoptotic form of the protein [60]. An important future direction
410 will be to examine whether NS1/2 interactions with the apoptotic machinery plays a role in
411 maintaining IEC infection.

412 As mentioned above, PS receptor activation associated with apoptotic death could limit
413 host responses. In contrast, virus production that results from cell lysis would promote
414 inflammatory signals to alert the host of an infection. In addition to professional phagocytes,
415 phagocytosis by non-professional phagocytes (e.g. epithelial cells) is critical for efficient clearance
416 of apoptotic cells, and for limiting inflammation in tissues with high cellular turnover [61].
417 Specifically, in a mouse model of colonic injury, phagocytic uptake of apoptotic cells by IECs was
418 sufficient for limiting inflammation in the colon [62], and phagocytosis mediated by epithelial cells
419 is similarly critical for reducing inflammation in lung tissue [63] and mammary glands [64]. Thus,
420 intestinal infection that promotes apoptotic death and the phagocytic uptake by IECs would limit
421 host detection and provide a non-inflammatory environment that would allow more efficient
422 infection of IECs and benefit MNV persistence. Future work will seek to identify the contribution
423 of these immunoregulatory pathways and apoptotic viral egress on IEC infection. Our discovery
424 of NS1/2 as an “apoptosis sensor” that reciprocally regulates apoptotic death and facilitates

425 epithelial spread (Fig. 11) has opened the door to such mechanistic studies and expanded our
426 understanding of the requirements for viral persistence in the intestine.

427 **Materials and Methods**

428 **Cells, virus, and plaque assays**

429 BV2 cells (gift from Herbert Virgin IV, Washington University, St. Louis, MO), a mouse
430 microglial cell line [65], were maintained in DMEM (Life Technologies, ThermoFisher, Carslbad,
431 CA) with 5% fetal bovine serum (FBS) (VWR Seradigm, Radnor, PA), 1X
432 Penicillin/Streptomycin/Glutamine (P/S/G) solution, and 10mM HEPES. M2C-CD300lf cells, a
433 murine colonic epithelial cell line transduced with the MNV receptor, CD300lf [28], were
434 maintained in DMEM with 10% FBS, 1X P/S/G, and 10mM HEPES. For bone-marrow derived
435 dendritic cells (BMDCs), bone marrow was isolated from the long bones of each hind leg of either
436 a WT or *Stat1*$^{-/-}$ mouse and suspended in RPMI (Life Technologies). Red blood cells were lysed
437 using red blood cell lysis solution (Sigma, St Louis, MO) and remaining bone marrow cells were
438 cultured in RPMI with 10% FBS, 1X P/S/G solution, 10mM HEPES, 1X Sodium Pyruvate, 1X non-
439 essential amino acids, and 20ng/mL GM-CSF obtained from supernatants of GM-CSF-secreting
440 cells (J558L, [66]). After seven days of culture (37C, 5% CO_2), non-adherent cells were collected,
441 infected in suspension with indicated MNV strains (MOI = 1), and plated without GM-CSF for the
442 indicated time. For indicated experiments, ZVAD-fmk (Cell Signaling Technology) was re-
443 suspended in DMSO and added to cells at 70 μM. As a positive control for apoptosis assays,
444 cells were treated with 1uM staurosporine (SS) (CST) for 3.5h, at 37C.

445 CR6$^{\Delta casp}$ MNV was generated using site directed mutagenesis as previously described [20]
446 with the following primers: CR6 $D_{121}G$, 5'-
447 GCCTAAGGAAGATAAAGCCG**G**TGCGCCCTCCCATGCG and CR6 $D_{131}G$, 5'-
448 TGCGGAGGACGCCATGG**G**TGCAAGGGAGCCCATAATTGG. The targeted residue is
449 underlined with the mutation in bold. Correct mutations were verified via sanger sequence
450 analysis.

451 MNV stocks were generated from plasmids, as described [22]. Briefly, plasmids encoding
452 viral genomes of parental CW3 (GenBank accession no. EF014462.1), parental CR6 (GenBank
453 accession no. JQ237823), CR6-VP1^{CW3} [20,22] and the two NS1/2$_{\Delta casp}$ viral genomes generated
454 herein, were individually transfected into 293T cells (ATCC #CRL-3216). Forty-eight hours post-
455 transfection, cells were frozen, thawed, vortexed, and spun at 3,000xg to remove large debris.
456 Supernatants were expanded by two passages at MOI <0.05 in BV2 cells, and p2 virus
457 supernatant was filtered (0.2 µm), concentrated by ultra-centrifugation through a 30% sucrose
458 cushion, and titered via plaque assay.
459 Plaque assays were performed in BV2 cells, similar to previously described methods [20].
460 Briefly, BV2 cells were grown in 6well plates, infected with serial dilutions of each sample (500ul
461 per well, 1h, RT, on a rocking platform), after which the inoculum was removed and cells were
462 overlaid with 1% methylcellulose in complete DMEM. At two to three days post-overlay, cells
463 were fixed and stained with 20% EtOH / 0.1% crystal violet.
464
465 **Incucyte live-cell imaging and analysis**
466 Cells were seeded in a 96-well plate, allowed to form a confluent monolayer (~18-24h), and
467 subsequently infected with MNV or UV-inactivated MNV (MOI=0.5). Mock-infected cells, and
468 cells treated with 1µM staurosporine were used for negative and positive controls, respectively.
469 Apoptosis and cell permeabilization were assessed via addition of Incucyte Annexin V Green
470 and Cytox Red reagents (EssenBioscience, Ann Arbor, MI), respectively, following manufacturer
471 protocols. Phase contrast and fluorescent images were collected with a 10x objective using the
472 IncuCyte Dual Dolor ZOOM (EssenBioscience) imaging system at 30minute intervals over a 72h
473 time course, maintained at 37°C and 5% CO_2. Images were analyzed using Incucyte 2016A
474 software (EssenBioscience) after Top-Hat background subtraction, with a 20µm radius.
475

476 **Mice, infections, and tissue collection**

477 *Stat1*$^{-/-}$ (*Stat1*^{tm1Dlv}) mice were originally obtained from the Jackson Laboratories (stock
478 #012606). *Ifnlr1*$^{-/-}$ (generated from *Ifnlr1*$^{tm1a(EUCOMM)Wtsi}$) and *Ifnar1*$^{-/-}$ (*Ifnar1*^{tm1Agt}) were originally
479 obtained from Washington University in St. Louis. *Ifnlr1*$^{-/-}$ and *Ifnar1*$^{-/-}$ were bred to generate *Ifnlr1*$^{-}$
480 $^{/-}$/*Ifnar1*$^{-/-}$ mice (DKO) and *Ifnlr1*$^{+/-}$/*Ifnar1*$^{+/-}$ (Dhet). Dhet and DKO crossbreeding yielded littermate
481 mice deficient in neither (Dhet), both (DKO), or a single (*Ifnlr1*$^{+/-}$/*Ifnar1*$^{-/-}$ or *Ifnlr1*$^{-/-}$/*Ifnar1*$^{+/-}$) IFN
482 receptor gene(s); these littermates were used for experiments to control for variability between
483 litters.

484 All mice (7-9weeks old) were perorally infected with 1e6 PFU in a 25µL volume
485 administered by pipet, with the exception of experiments in Figure 5 where 1e6 or 1e7 PFU (as
486 indicated in figure) was administered by oral gavage in a 100µL volume. An equal proportion of
487 males and females were maintained among experimental groups to mitigate results due to any
488 unidentified sex-dependent variables. Same-sex mice, infected with the same MNV strain, were
489 often co-housed for acute infection analyses (less than three days), but singly-housed for
490 extended experiments to prevent continued transmission between animals.

491 Tissue samples, or a single fecal pellet, were collected in 2ml cryovials with 1mm
492 zirconia/silica beads (Biospec, Bartlesville, OK), frozen in a dry ice/EtOH bath and stored at -80C.
493 For plaque assay or RT-qPCR analyses, either 1ml DMEM or 1ml RiboZol (VWR) was added,
494 respectively, and tissues were homogenized via bead-beating (1min, RT) prior to continued
495 analysis.

496

497 **Ethics Statement**

498 All mice were bred on C57BL/6 background and maintained in specific-pathogen-free
499 barrier facilities at Oregon Health & Science University under animal protocols approved by the

500 institutional animal care and use committee at Oregon Health & Science University (protocol #
501 IP00000228) according to standards set forth in the *Animal Welfare Act*.
502
503 **RNA, cDNA, and RT-qPCR**
504 RNA from tissues was extracted via RiboZol (VWR) protocols, and RNA from cells was
505 extracted with the ZR Viral RNA kit (Zymoresearch, Irvine, CA). DNA contamination was
506 removed with Turbo DNase (ThermoFisher), and 1ug of RNA was used to generate cDNA with
507 the ImpromII reverse transcriptase (Promega, Madison, WI). Quantitative PCR was performed
508 using PerfeCTa qPCR FastMix II (QuantaBio, Beverly, MA), and the following oligo/probes were
509 used for detection: MNV genomic RNA - Forward primer CACGCCACCGATCTGTTCTG,
510 Reverse primer GCGCTGCGCCATCACTC, and Probe TGCGCTTTGGAACAATGG; RPS29 -
511 Forward primer GCAAATACGGGCTGAACATG, Reverse primer GTCCAACTTAATG
512 AAGCCTATGTC, and Probe CCTTCGCGTACTGCCGGAAGC.
513
514 **Cell Lysates and Western blot**
515 BV2 cells were grown and infected in 12well plates (2 e5 cells/well). Cells were lifted with
516 trypsin/0.25% EDTA (Gibco, ThermoFisher), washed with 1X cold PBS, resuspended in 100 µL
517 NP40 lysis buffer (Alfo Aesar, Havervill, MA) with protease inhibitor cocktail (Sigma, St Louis,
518 MO), incubated on ice (15min with intermittent mixing), cleared via centrifugation (1min, 4C, full-
519 speed), and diluted 1:1 with 2x SDS loading buffer (0.125 M Tris [pH 6.8], 4% SDS, 20% glycerol,
520 0.004% bromophenol blue, 10% beta-mercaptoethanol). Lysates were run on Novex Tris-Glycine
521 gels (ThermoFisher), transferred to 0.2 µm PVDF (BioRad, Hercules, CA), blocked with 5% nonfat
522 dry milk, and probed with the following antibodies (Ab): caspase 3 (CST), PARP (CST), beta-
523 Actin pAb (Invitrogen), MNV NS1/2 (a gift from Dr. Vernon Ward, U. of Otago, Australia), or MNV
524 ProPol (a gift form Dr. Kim Green, NIH). Signal was detected using goat, anti-rabbit IgG-HRP

525 (Jackson ImmunoResearch), developed with ECL substrate (Pierce, ThermoFisher), and imaged
526 with an ImageQuant LAS4000 (GE Healthcare, Little Chalfont, UK).
527
528 **Intestinal epithelial cell collection**

529 Epithelial fractions were prepared by non-enzymatic striping as previously described [31].
530 Mice were euthanized and distal small intestine, cecum, and colon (regions of highest MNV
531 replication) were isolated. Peyer's patches were removed from small intestine and intestinal
532 tissues were incubated in stripping buffer (10% bovine calf serum, 15 mM HEPES, 5 mM EDTA,
533 5 mM dithiothreitol [DTT] in PBS) with shaking for 20 min at 37°C. The dissociated cells were
534 collected as the epithelial fraction, consisting predominantly of IECs and directly used for flow
535 cytometry.

536
537 **Surface and intracellular staining and flow cytometry**
538 BV2 cells were trypsinized and washed once with 1X PBS, stained with the amine-reactive
539 viability dye, Zombie Aqua (Biolegend, San Diego, CA) (20min, on ice), washed once with cold
540 2% FBS/PBS, washed once with cold Annexin V binding buffer (CST), and stained with Annexin
541 V-FITC (CST) (15min, RT). Cells were immediately analyzed via flow cytometry on an LSR
542 Fortessa (Becton Dickinson [BD], Franklin Lakes, NJ) with FACSDiva software (BD), and data
543 was analyzed using FlowJo software (FlowJo LLC, Ashland, OR).
544 IECs isolated as described above were stained with the Zombie Aqua viability dye
545 (Biolegend), Fc receptors were blocked with purified CD16/CD32 pAb (clone93; Biolegend), and
546 cells were probed for surface markers, EpCAM (clone G8.8; Biolegend) and CD45 (clone 30-F11;
547 Biolegend). Cells were subsequently fixed with 2% paraformaldehyde/PBS (10min, RT), and
548 blocked/permeablized in 0.2% Triton X/PBS with 2% normal goat serum (20min, RT). Fixed and

549 permeabilized cells were probed for intracellular viral antigen with 2 distinct antibodies: Rabbit
550 polyclonal anti-NS1/2 (a gift from Dr. Vernon Ward, U. of Otago, Australia) and mouse monoclonal
551 anti-NS1 (clone CM79, a gift from Dr. Ian Clark, U. of Southampton, UK). These unconjugated
552 antibodies were detected with anti-Rabbit Alexa Fluor 647 (Molecular Probes, Eugene, OR), and
553 anti-mouse Dylight 405 (Jackson ImmunoResearch), respectively. Cells were analyzed via flow
554 cytometry, and viable cells that were EpCAM+, CD45-, NS1/2 pAb+, and NS1 mAb+ were labeled
555 as infected epithelial cells.
556
557 **RNA *in situ* hybridization via RNAscope®**
558 Ileum was opened longitudinally, pinned apical side up in wax trays, and fixed in 10%
559 neutral-buffered formalin (Sigma) (18-24h, RT), then moved to 70% EtOH. Tissues were
560 embedded in 2% agar (ThermoFisher), the PP was vertically transected, flipped 90 degrees, and
561 re-embedded in 2% agar. Agar blocks were maintained in 70% EtOH prior to being paraffin-
562 embedded. Tissue sections (5um) were cut and maintained at RT with desiccant until processed.
563 RNA *in situ* hybridization was performed using the RNAscope Multiplex Fluorescent v2 kit
564 (Advanced Cell Diagnostics [ACDBio], Newark, CA) per protocol guidelines. Probes were
565 designed by ACDBio for detection of CW3 positive strand RNA (471891-C1), CR6 positive strand
566 RNA (502631-C1), and EpCAM mRNA (418151-C2), and signals were amplified and detected via
567 ACDBio protocols using TSA® plus technology (Perkin Elmer, Waltham, MA). Slides were
568 mounted with ProLong Gold antifade reagent (ThermoFisher), and imaged using a Zeiss
569 ApoTome2 on an Axio Imager, with a Zeiss AxioCam 506 (Zeiss, Jena, Germany).
570
571 **Statistical Analyses**
572 Data were analyzed with Prism 7 software (GraphPad Prism Software, La Jolla, CA), with
573 specified tests and significance noted in the figure legends.

Acknowledgements:

The authors would like to thank the OHSU Advanced Light Microscopy Core, Flow Cytometry Core, and Histopathology Shared Resource for technical support, Lena Li for overseeing mouse colonies, and Stephanie Karst for guidance with RNAscope techniques.

579 1. Ahmed SM, Hall AJ, Robinson AE, Verhoef L, Premkumar P, Parashar UD, et al. Global
580 prevalence of norovirus in cases of gastroenteritis: a systematic review and meta-
581 analysis. Lancet Infect Dis. World Health Organization. Published by Elsevier Ltd/Inc/BV.
582 All rights reserved.; 2014;14: 725–730. doi:10.1016/S1473-3099(14)70767-4
583 2. Glass RI, Parashar UD, Estes MK. Norovirus gastroenteritis. N Engl J Med. 2009;361:
584 1776–85. doi:10.1056/NEJMra0804575
585 3. Saito M, Goel-Apaza S, Espetia S, Velasquez D, Cabrera L, Loli S, et al. Multiple
586 Norovirus Infections in a Birth Cohort in a Peruvian Periurban Community. Clin Infect Dis.
587 2014;58: 483–491. doi:10.1093/cid/cit763
588 4. Teunis PFM, Sukhrie FHA, Vennema H, Bogerman J, Beersma MFC, Koopmans MPG.
589 Shedding of norovirus in symptomatic and asymptomatic infections. Epidemiol Infect.
590 2015;143: 1710–7. doi:10.1017/S095026881400274X
591 5. Ettayebi K, Crawford SE, Murakami K, Broughman JR, Karandikar U, Tenge VR, et al.
592 Replication of human noroviruses in stem cell-derived human enteroids. Science.
593 2016;353: 1387–1393. doi:10.1126/science.aaf5211
594 6. Jones MK, Watanabe M, Zhu S, Graves CL, Keyes LR, Grau KR, et al. Enteric bacteria
595 promote human and mouse norovirus infection of B cells. Science. 2014;346: 755–9.
596 doi:10.1126/science.1257147
597 7. Karst SM, Wobus CE. A Working Model of How Noroviruses Infect the Intestine. Rall GF,
598 editor. PLOS Pathog. 2015;11: e1004626. doi:10.1371/journal.ppat.1004626
599 8. Nice TJ, Robinson BA, Van Winkle JA. The Role of Interferon in Persistent Viral Infection:
600 Insights from Murine Norovirus. Trends Microbiol. Elsevier Ltd; 2018;26: 510–524.
601 doi:10.1016/j.tim.2017.10.010
602 9. Baldridge MT, Turula H, Wobus CE. Norovirus Regulation by Host and Microbe. Trends
603 Mol Med. 2016;22: 1047–1059. doi:10.1016/j.molmed.2016.10.003

604 10. Karst SM, Wobus CE, Lay M, Davidson J, Virgin HW. STAT1-dependent innate immunity
605 to a Norwalk-like virus. Science. 2003;299: 1575–8. doi:10.1126/science.1077905
606 11. Lambden PR, Caul EO, Ashley CR, Clarke IN. Sequence and genome organization of a
607 human small round-structured (Norwalk-like) virus. Science. 1993;259: 516–9. Available:
608 http://www.ncbi.nlm.nih.gov/pubmed/8380940
609 12. Sosnovtsev S V, Belliot G, Chang K-O, Prikhodko VG, Thackray LB, Wobus CE, et al.
610 Cleavage Map and Proteolytic Processing of the Murine Norovirus Nonstructural
611 Polyprotein in Infected Cells. J Virol. 2006;80: 7816–7831. doi:10.1128/JVI.00532-06
612 13. Seah EL, Marshall JA, Wright PJ. trans activity of the norovirus Camberwell proteinase
613 and cleavage of the N-terminal protein encoded by ORF1. J Virol. 2003;77: 7150–7155.
614 doi:10.1128/JVI.77.12.7150
615 14. Liu B, Clarke IN, Lambden PR. Polyprotein processing in Southampton virus: identification
616 of 3C-like protease cleavage sites by in vitro mutagenesis. J Virol. 1996;70: 2605–10.
617 Available: http://www.ncbi.nlm.nih.gov/pubmed/8642693
618 15. Hyde JL, Sosnovtsev S V, Green KY, Wobus C, Virgin HW, Mackenzie JM. Mouse
619 Norovirus Replication Is Associated with Virus-Induced Vesicle Clusters Originating from
620 Membranes Derived from the Secretory Pathway. J Virol. 2009;83: 9709–9719.
621 doi:10.1128/JVI.00600-09
622 16. Hyde JL, Mackenzie JM. Subcellular localization of the MNV-1 ORF1 proteins and their
623 potential roles in the formation of the MNV-1 replication complex. Virology. 2010;406:
624 138–148. doi:10.1016/j.virol.2010.06.047
625 17. Doerflinger SY, Cortese M, Romero-Brey I, Menne Z, Tubiana T, Schenk C, et al.
626 Membrane alterations induced by nonstructural proteins of human norovirus. PLoS
627 Pathog. 2017;13: e1006705. doi:10.1371/journal.ppat.1006705
628 18. Ettayebi K, Hardy ME. Norwalk Virus Nonstructural Protein p48 Forms a Complex with the

629 SNARE Regulator VAP-A and Prevents Cell Surface Expression of Vesicular Stomatitis
630 Virus G Protein. J Virol. 2003;77: 11790–11797. doi:10.1128/JVI.77.21.11790-11797.2003
631 19. Thorne LG, Goodfellow IG. Norovirus gene expression and replication. J Gen Virol.
632 2014;95: 278–291. doi:10.1099/vir.0.059634-0
633 20. Nice TJ, Strong DW, McCune BT, Pohl CS, Virgin HW. A single-amino-acid change in
634 murine norovirus NS1/2 is sufficient for colonic tropism and persistence. J Virol. 2013;87:
635 327–34. doi:10.1128/JVI.01864-12
636 21. Bailey D, Thackray LB, Goodfellow IG. A Single Amino Acid Substitution in the Murine
637 Norovirus Capsid Protein Is Sufficient for Attenuation In Vivo. J Virol. 2008;82: 7725–
638 7728. doi:10.1128/JVI.00237-08
639 22. Strong DW, Thackray LB, Smith TJ, Virgin HW. Protruding domain of capsid protein is
640 necessary and sufficient to determine murine norovirus replication and pathogenesis in
641 vivo. J Virol. 2012;86: 2950–8. doi:10.1128/JVI.07038-11
642 23. Wobus CE, Karst SM, Thackray LB, Chang K-O, Sosnovtsev S V., Belliot G, et al.
643 Replication of Norovirus in Cell Culture Reveals a Tropism for Dendritic Cells and
644 Macrophages. Michael Emerman, editor. PLoS Biol. 2004;2: e432.
645 doi:10.1371/journal.pbio.0020432
646 24. Grau KR, Roth AN, Zhu S, Hernandez A, Colliou N, DiVita BB, et al. The major targets of
647 acute norovirus infection are immune cells in the gut-associated lymphoid tissue. Nat
648 Microbiol. 2017;2: 1586–1591. doi:10.1038/s41564-017-0057-7
649 25. Orchard RC, Wilen CB, Doench JG, Baldridge MT, McCune BT, Lee Y-CJ, et al.
650 Discovery of a proteinaceous cellular receptor for a norovirus. Science. 2016;353: 933–6.
651 doi:10.1126/science.aaf1220
652 26. Haga K, Fujimoto A, Takai-Todaka R, Miki M, Doan YH, Murakami K, et al. Functional
653 receptor molecules CD300lf and CD300ld within the CD300 family enable murine

654 noroviruses to infect cells. Proc Natl Acad Sci U S A. 2016;113: E6248–E6255.
655 doi:10.1073/pnas.1605575113
656 27. Wilen CB, Lee S, Hsieh LL, Orchard RC, Desai C, Hykes BL, et al. Tropism for tuft cells
657 determines immune promotion of norovirus pathogenesis. Science. 2018;360: 204–208.
658 doi:10.1126/science.aar3799
659 28. Lee S, Wilen CB, Orvedahl A, McCune BT, Kim K-W, Orchard RC, et al. Norovirus Cell
660 Tropism Is Determined by Combinatorial Action of a Viral Non-structural Protein and Host
661 Cytokine. Cell Host Microbe. 2017;22: 449–459.e4. doi:10.1016/j.chom.2017.08.021
662 29. Haber AL, Biton M, Rogel N, Herbst RH, Shekhar K, Smillie C, et al. A single-cell survey
663 of the small intestinal epithelium. Nature. Nature Publishing Group; 2017;551: 333–339.
664 doi:10.1038/nature24489
665 30. Hoffmann H-H, Schneider WM, Rice CM. Interferons and viruses: an evolutionary arms
666 race of molecular interactions. Trends Immunol. 2015;36: 124–38.
667 doi:10.1016/j.it.2015.01.004
668 31. Nice TJ, Osborne LC, Tomov VT, Artis D, Wherry EJJ, Virgin HW. Type I Interferon
669 Receptor Deficiency in Dendritic Cells Facilitates Systemic Murine Norovirus Persistence
670 Despite Enhanced Adaptive Immunity. Coyne CB, editor. PLoS Pathog. 2016;12:
671 e1005684. doi:10.1371/journal.ppat.1005684
672 32. Thackray LB, Duan E, Lazear HM, Kambal A, Schreiber RD, Diamond MS, et al. Critical
673 Role for Interferon Regulatory Factor 3 (IRF-3) and IRF-7 in Type I Interferon-Mediated
674 Control of Murine Norovirus Replication. J Virol. 2012;86: 13515–13523.
675 doi:10.1128/JVI.01824-12
676 33. Baldridge MT, Nice TJ, McCune BT, Yokoyama CC, Kambal A, Wheadon M, et al.
677 Commensal microbes and interferon-λ determine persistence of enteric murine norovirus
678 infection. Science. 2015;347: 266–9. doi:10.1126/science.1258025

679 34. Nice TJ, Baldridge MT, McCune BT, Norman JM, Lazear HM, Artyomov M, et al.
680 Interferon-λ cures persistent murine norovirus infection in the absence of adaptive
681 immunity. Science. 2015;347: 269–73. doi:10.1126/science.1258100
682 35. Taylor RC, Cullen SP, Martin SJ. Apoptosis: controlled demolition at the cellular level. Nat
683 Rev Mol Cell Biol. 2008;9: 231–41. doi:10.1038/nrm2312
684 36. Polster BM, Pevsner J, Hardwick JM. Viral Bcl-2 homologs and their role in virus
685 replication and associated diseases. Biochim Biophys Acta. 2004;1644: 211–27.
686 doi:10.1016/j.bbamcr.2003.11.001
687 37. Galluzzi L, Brenner C, Morselli E, Touat Z, Kroemer G. Viral control of mitochondrial
688 apoptosis. PLoS Pathog. 2008;4. doi:10.1371/journal.ppat.1000018
689 38. Amara A, Mercer J. Viral apoptotic mimicry. Nat Rev Microbiol. Nature Publishing Group;
690 2015;13: 461–469. doi:10.1038/nrmicro3469
691 39. Richard A, Tulasne D. Caspase cleavage of viral proteins, another way for viruses to
692 make the best of apoptosis. Cell Death Dis. 2012;3: e277. doi:10.1038/cddis.2012.18
693 40. Mebratu YA, Tipper J, Chand HS, Walton S, Harrod KS, Tesfaigzi Y. Bik Mediates
694 Caspase-Dependent Cleavage of Viral Proteins to Promote Influenza A Virus Infection.
695 Am J Respir Cell Mol Biol. 2016;54: 664–73. doi:10.1165/rcmb.2015-0133OC
696 41. Al-Molawi N, Beardmore VA, Carter MJ, Kass GEN, Roberts LO. Caspase-mediated
697 cleavage of the feline calicivirus capsid protein. J Gen Virol. 2003;84: 1237–44.
698 doi:10.1099/vir.0.18840-0
699 42. Cheetham S, Souza M, Meulia T, Grimes S, Han MG, Saif LJ. Pathogenesis of a
700 genogroup II human norovirus in gnotobiotic pigs. J Virol. 2006;80: 10372–81.
701 doi:10.1128/JVI.00809-06
702 43. Troeger H, Loddenkemper C, Schneider T, Schreier E, Epple H-J, Zeitz M, et al.
703 Structural and functional changes of the duodenum in human norovirus infection. Gut.

704 2009;58: 1070–7. doi:10.1136/gut.2008.160150
705 44. Mumphrey SM, Changotra H, Moore TN, Heimann-Nichols ER, Wobus CE, Reilly MJ, et
706 al. Murine norovirus 1 infection is associated with histopathological changes in
707 immunocompetent hosts, but clinical disease is prevented by STAT1-dependent interferon
708 responses. J Virol. 2007;81: 3251–3263. doi:10.1128/JVI.02096-06
709 45. Bok K, Prikhodko VG, Green KY, Sosnovtsev S V. Apoptosis in Murine Norovirus-Infected
710 RAW264.7 Cells Is Associated with Downregulation of Survivin. J Virol. 2009;83: 3647–
711 3656. doi:10.1128/JVI.02028-08
712 46. Furman LM, Maaty WS, Petersen LK, Ettayebi K, Hardy ME, Bothner B. Cysteine
713 protease activation and apoptosis in Murine norovirus infection. Virol J. 2009;6: 139.
714 doi:10.1186/1743-422X-6-139
715 47. Herod MR, Salim O, Skilton RJ, Prince CA, Ward VK, Lambden PR, et al. Expression of
716 the Murine Norovirus (MNV) ORF1 Polyprotein Is Sufficient to Induce Apoptosis in a
717 Virus-Free Cell Model. PLoS One. 2014;9: e90679. doi:10.1371/journal.pone.0090679
718 48. Van Winkle JA, Robinson BA, Peters AM, Li L, Nouboussi R V, Mack M, et al. Persistence
719 of Systemic Murine Norovirus Is Maintained by Inflammatory Recruitment of Susceptible
720 Myeloid Cells. Cell Host Microbe. 2018;24: 665–676.e4. doi:10.1016/j.chom.2018.10.003
721 49. Chang HY, Yang X. Proteases for cell suicide: functions and regulation of caspases.
722 Microbiol Mol Biol Rev. 2000;64: 821–46. Available:
723 http://www.ncbi.nlm.nih.gov/pubmed/11104820
724 50. McCune BT, Tang W, Lu J, Eaglesham JB, Thorne L, Mayer AE, et al. Noroviruses Co-opt
725 the Function of Host Proteins VAPA and VAPB for Replication via a Phenylalanine-
726 Phenylalanine-Acidic-Tract-Motif Mimic in Nonstructural Viral Protein NS1/2. Dermody TS,
727 editor. MBio. 2017;8: 1–17. doi:10.1128/mBio.00668-17
728 51. Feng Z, Hensley L, McKnight KL, Hu F, Madden V, Ping L, et al. A pathogenic

729 picornavirus acquires an envelope by hijacking cellular membranes. Nature. Nature
730 Publishing Group; 2013;496: 367–71. doi:10.1038/nature12029
731 52. Chen Y-H, Du W, Hagemeijer MC, Takvorian PM, Pau C, Cali A, et al. Phosphatidylserine
732 Vesicles Enable Efficient En Bloc Transmission of Enteroviruses. Cell. 2015;160: 619–
733 630. doi:10.1016/j.cell.2015.01.032
734 53. Bhattacharyya S, Zagórska A, Lew ED, Shrestha B, Rothlin C V, Naughton J, et al.
735 Enveloped viruses disable innate immune responses in dendritic cells by direct activation
736 of TAM receptors. Cell Host Microbe. 2013;14: 136–47. doi:10.1016/j.chom.2013.07.005
737 54. Santiana M, Ghosh S, Ho BA, Rajasekaran V, Du WL, Mutsafi Y, et al. Vesicle-Cloaked
738 Virus Clusters Are Optimal Units for Inter-organismal Viral Transmission. Cell Host
739 Microbe. 2018; 208–220. doi:10.1016/j.chom.2018.07.006
740 55. Gerbe F, Sidot E, Smyth DJ, Ohmoto M, Matsumoto I, Dardalhon V, et al. Intestinal
741 epithelial tuft cells initiate type 2 mucosal immunity to helminth parasites. Nature. Nature
742 Publishing Group, a division of Macmillan Publishers Limited. All Rights Reserved.;
743 2016;529: 226. Available: https://doi.org/10.1038/nature16527
744 56. Von Moltke J, Ji M, Liang HE, Locksley RM. Tuft-cell-derived IL-25 regulates an intestinal
745 ILC2-epithelial response circuit. Nature. Nature Publishing Group; 2016;529: 221–225.
746 doi:10.1038/nature16161
747 57. Delgado ME, Grabinger T, Brunner T. Cell death at the intestinal epithelial front line.
748 FEBS J. 2016;283: 2701–19. doi:10.1111/febs.13575
749 58. Reginato MJ, Mills KR, Paulus JK, Lynch DK, Sgroi DC, Debnath J, et al. Integrins and
750 EGFR coordinately regulate the pro-apoptotic protein Bim to prevent anoikis. Nat Cell Biol.
751 2003;5: 733–40. doi:10.1038/ncb1026
752 59. Hausmann M, Leucht K, Ploner C, Kiessling S, Villunger A, Becker H, et al. BCL-2
753 modifying factor (BMF) is a central regulator of anoikis in human intestinal epithelial cells.

754 J Biol Chem. 2011;286: 26533–40. doi:10.1074/jbc.M111.265322
755 60. Youle RJ, Strasser A. The BCL-2 protein family: opposing activities that mediate cell
756 death. Nat Rev Mol Cell Biol. 2008;9: 47–59. doi:10.1038/nrm2308
757 61. Poon IKH, Lucas CD, Rossi AG, Ravichandran KS. Apoptotic cell clearance: basic biology
758 and therapeutic potential. Nat Rev Immunol. Nature Publishing Group; 2014;14: 166–180.
759 doi:10.1038/nri3607
760 62. Lee CS, Penberthy KK, Wheeler KM, Juncadella IJ, Vandenabeele P, Lysiak JJ, et al.
761 Boosting Apoptotic Cell Clearance by Colonic Epithelial Cells Attenuates Inflammation In
762 Vivo. Immunity. Elsevier Inc.; 2016;44: 807–20. doi:10.1016/j.immuni.2016.02.005
763 63. Juncadella IJ, Kadl A, Sharma AK, Shim YM, Hochreiter-Hufford A, Borish L, et al.
764 Apoptotic cell clearance by bronchial epithelial cells critically influences airway
765 inflammation. Nature. 2013;493: 547–51. doi:10.1038/nature11714
766 64. Monks J, Rosner D, Geske FJ, Lehman L, Hanson L, Neville MC, et al. Epithelial cells as
767 phagocytes: apoptotic epithelial cells are engulfed by mammary alveolar epithelial cells
768 and repress inflammatory mediator release. Cell Death Differ. 2005;12: 107–14.
769 doi:10.1038/sj.cdd.4401517
770 65. Blasi E, Barluzzi R, Bocchini V, Mazzolla R, Bistoni F. Immortalization of murine microglial
771 cells by a v-raf/v-myc carrying retrovirus. J Neuroimmunol. Netherlands; 1990;27: 229–37.
772 Available: http://www.ncbi.nlm.nih.gov/pubmed/2110186
773 66. Qin Z, Noffz G, Mohaupt M, Blankenstein T. Interleukin-10 prevents dendritic cell
774 accumulation and vaccination with granulocyte-macrophage colony-stimulating factor
775 gene-modified tumor cells. J Immunol. 1997;159: 770–6. Available:
776 http://www.jimmunol.org/content/159/2/770.abstract
777 67. Gonzalez-Hernandez MB, Liu T, Payne HC, Stencel-Baerenwald JE, Ikizler M, Yagita H,
778 et al. Efficient Norovirus and Reovirus Replication in the Mouse Intestine Requires

779 Microfold (M) Cells. J Virol. 2014;88: 6934–6943. doi:10.1128/JVI.00204-14

780

781

Figure 1

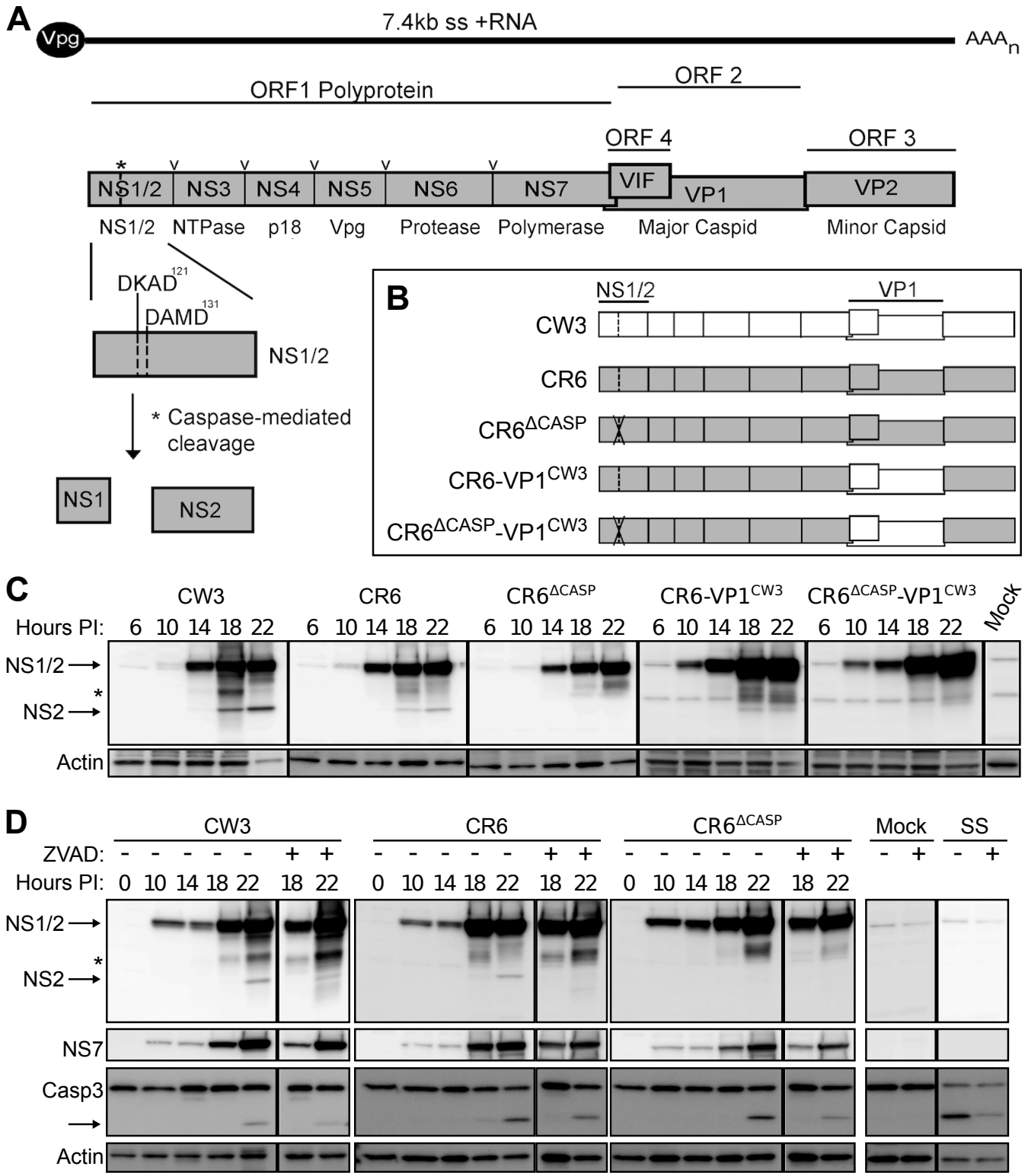

Fig. 1. MNV NS1/2 is cleaved by host caspases at late times-post-infection. (A) Schematic of MNV genomic organization, illustrating initial NS1/2 expression within the ORF1 polyprotein. Sites indicated in ORF1 are cleaved by the viral protease (**v**) and host caspases (*****), the latter at

786 aspartic acid residues 121 and 131 within two caspase motifs, DKAD^{121} and DAMD^{131}. (B)
787 Schematic representation of the five MNV clones used in these studies. D121G and D131G
788 mutations are indicated by the X within NS1/2. (C) BV2 cells were infected with indicated strains
789 of MNV (MOI=1), and whole cell extracts (WCE) were analyzed via western blot (WB) at indicated
790 times post-infection. Image is representative of 4 independent experiments. Arrows indicate full-
791 length NS1/2 (45kD) and NS2 (28kD). * Denotes caspase-independent bands >28kD. (D) BV2
792 cells were infected as in C, but subsequently treated with 50uM ZVAD-fmk at 10 hours post-
793 infection, and WCE were probed for NS1/2, NS7, caspase 3, and actin via WB. Image is
794 representative of 3 independent experiments. SS = staurosporine.
795

Figure 2

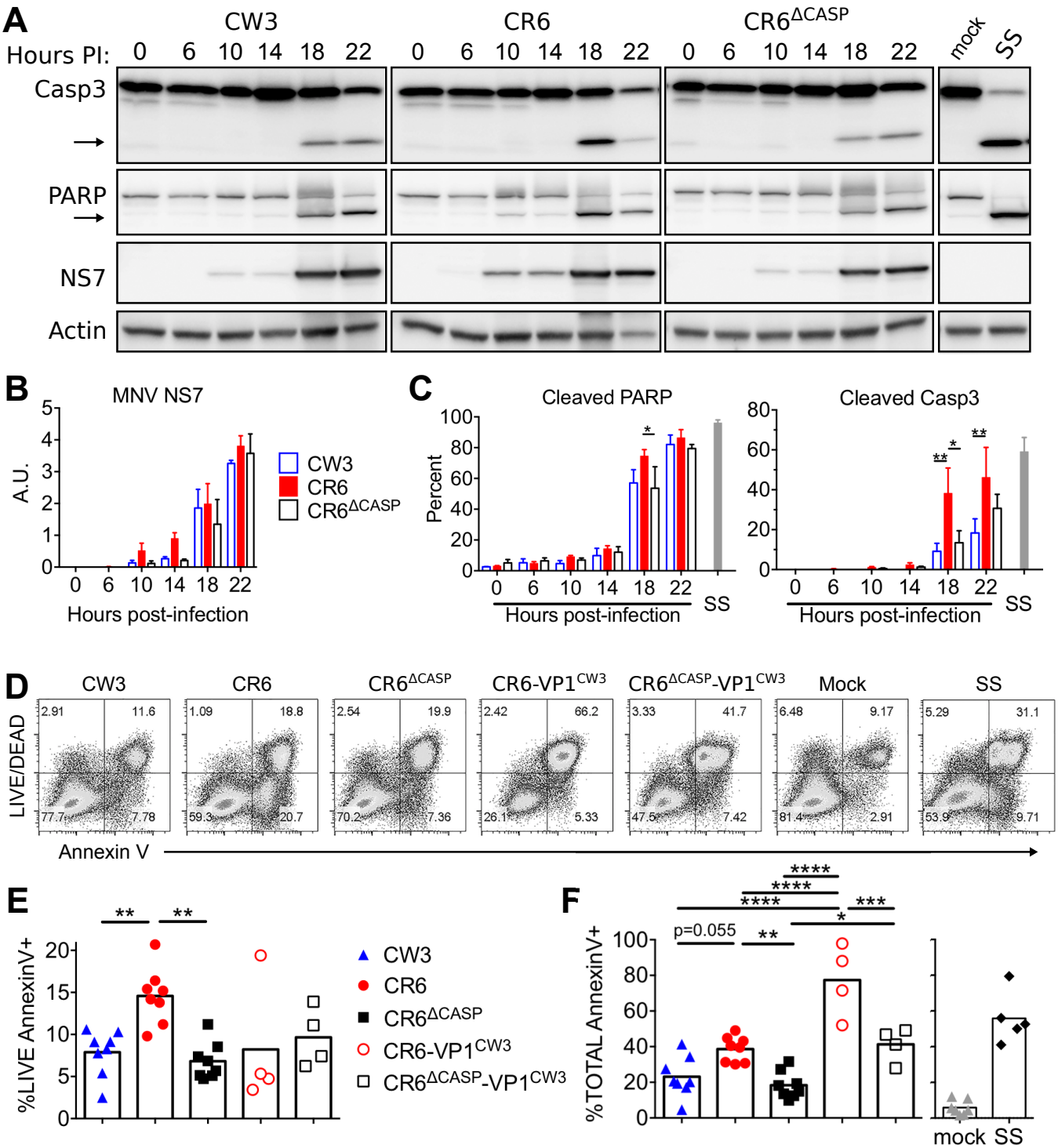

Fig. 2. Cleavage of NS1/2 promotes apoptosis of myeloid cells. BV2 cells were infected (MOI=1) with indicated MNV strains. (A-C) Whole cell extracts were collected at indicated times and analyzed via WB for caspase 3, PARP, actin, and MNV NS7. (A) Arrows denote cleaved fragments of caspase 3 and PARP. Images are representative of three independent experiments.

801 (B) NS7 normalized to actin analyzed via densitometry. (C) Cleaved PARP and Caspase 3 were
802 quantified as a proportion of total protein by densitometry. (D-F) Cells were harvested at 17 hours
803 post-infection, stained with Annexin V and LIVE/DEAD viability stain, and analyzed via flow
804 cytometry. (D) Representative flow plots are shown from one of eight independent experiments.
805 (E) Live, Annexin V+, and (F) total Annexin V+ cells from all experiments are graphed and mean
806 values are indicated. Statistical significance was determined by one-way (E-F) or two-way (B-C)
807 ANOVA, with Tukey's multiple comparison test. *, $p \leq 0.05$; **, $p \leq 0.01$; ***, $p \leq 0.001$; ****, $p \leq$
808 0.0001; SS, staurosporine.

809

Figure 3

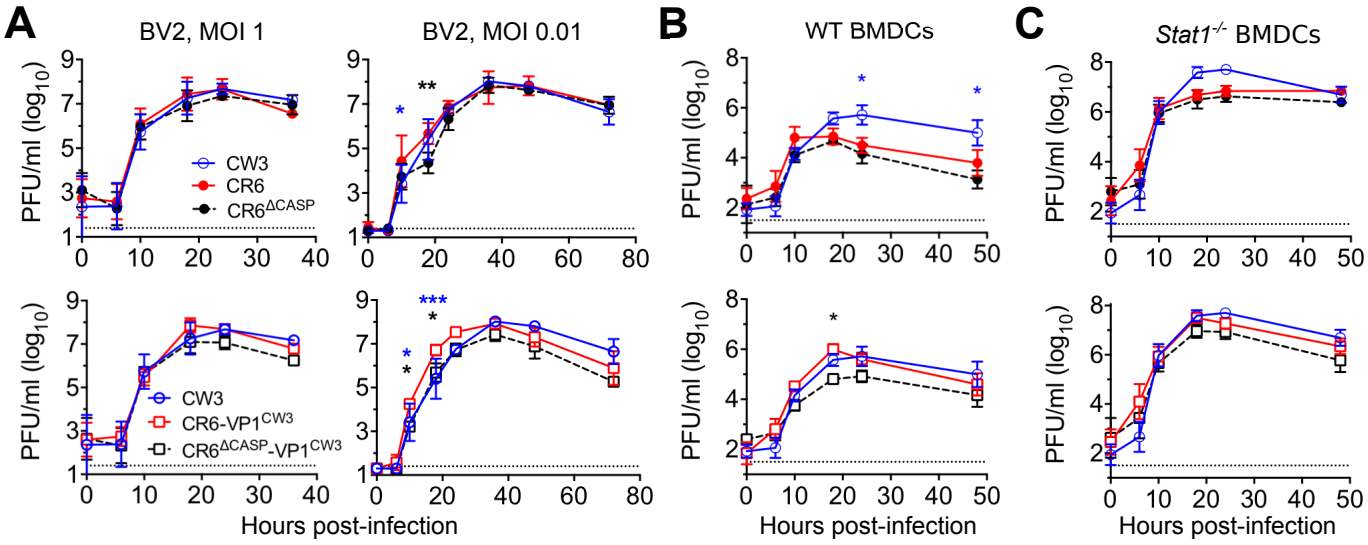

810

811 **Fig. 3. Cleavage of NS1/2 is not required for *in vitro* MNV replication in myeloid cells.** BV2
812 cells (A), WT BMDCs (B), or *Stat1*$^{-/-}$ BMDCs (C) were infected with the indicated strain of MNV at
813 MOI 0.01 (A) or MOI 1 (A-C) and infectious virus was analyzed at indicated times post-infection
814 via plaque assay. Dotted lines indicate limit of detection. Error bars indicate SEM. Statistical
815 significance was determined via two-way ANOVA with Tukey's multiple comparisons test. *, $p \leq$
816 0.05; **, $p \leq 0.01$. BMDCs = bone marrow-derived dendritic cells. Data are an average of at least
817 three independent experiments.

Figure 4

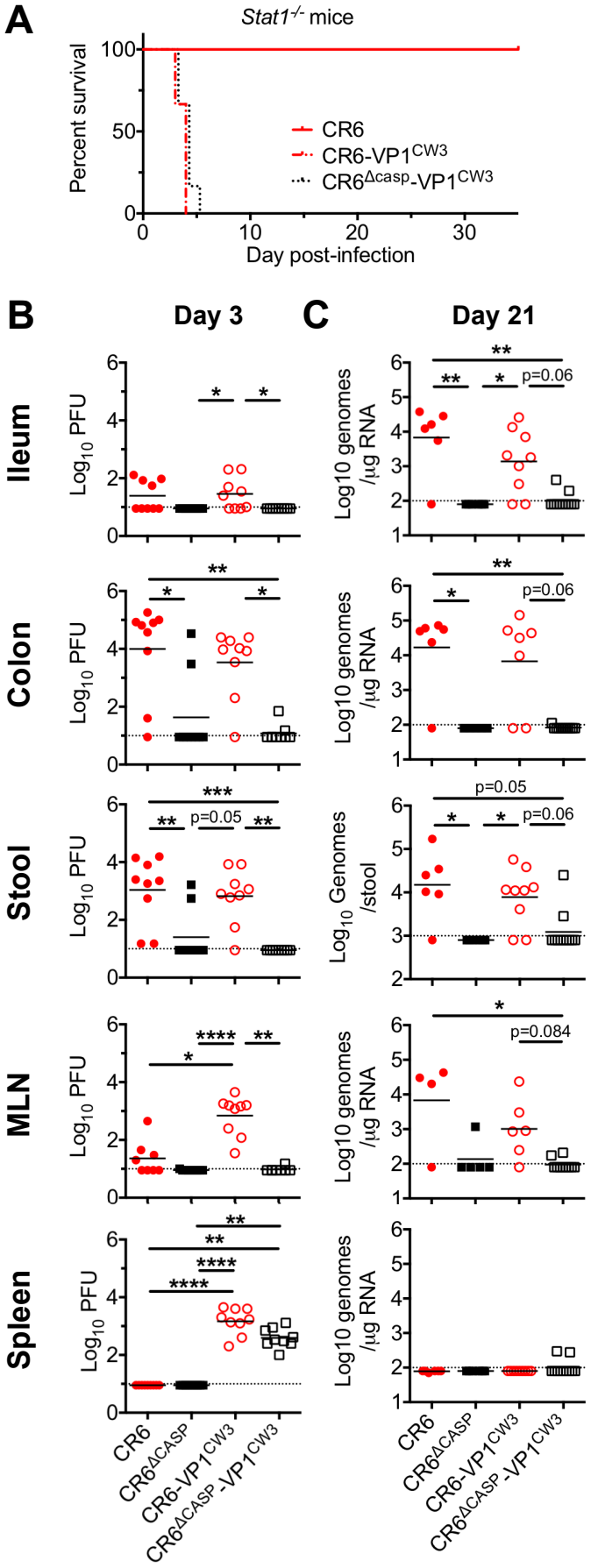
A
Stat1-/- mice
Percent survival
100
50
0
0
10
20
30
Day post-infection
CR6
CR6-VP1CW3
CR6ΔCASP-VP1CW3
B
Day 3
C
Day 21
Ileum
Colon
Stool
MLN
Spleen
Log10 PFU
Log10 genomes /µg RNA
Log10 Genomes /stool
p=0.06
p=0.05
p=0.084
CR6
CR6ΔCASP
CR6-VP1CW3
CR6ΔCASP-VP1CW3

818

819 **Fig. 4. NS1/2 cleavage is required for intestinal tropism and persistence**. (A) *Stat1*$^{-/-}$ mice
820 were infected with the indicated strain and monitored daily for lethality. (B-C) WT mice were
821 perorally infected with indicated viruses (1e6 PFU). At 3 (B) or 21 (C) days post-infection, tissues
822 and stool were harvested and analyzed via plaque assay (B) or qPCR (D). Data are from 8-9
823 individual mice combined from 3 separate experiments, and mean values are indicated. Statistical
824 significance was determined by Kruskal-Wallis test. *, $p \leq 0.05$; **, $p \leq 0.01$; ***, $p \leq 0.001$; ****,
825 $p \leq 0.0001$; MLN, mesenteric lymph node.

826

827

Figure 5

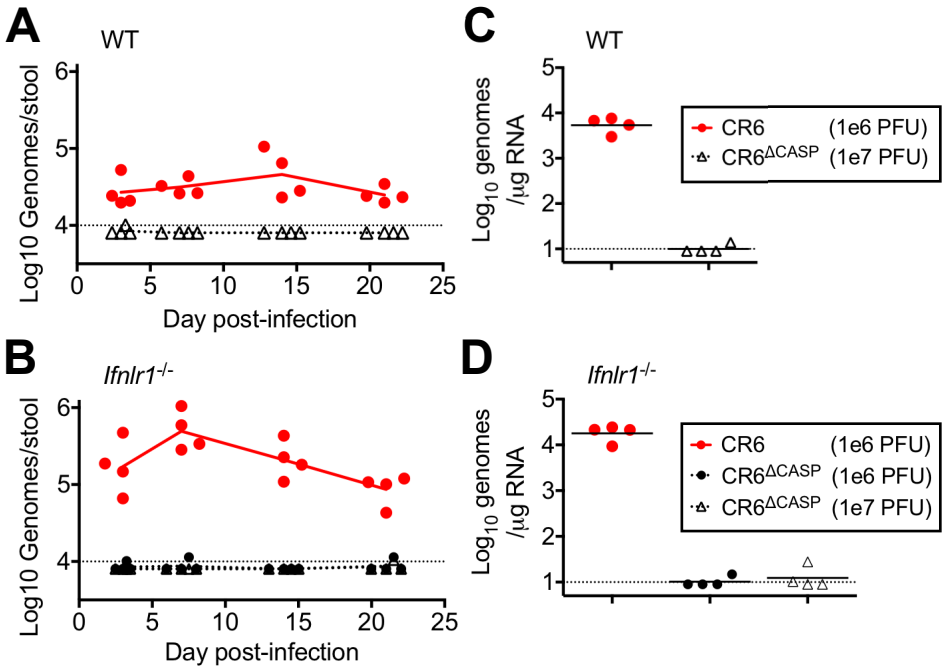

828

829 **Fig. 5. Caspase cleavage of NS1/2 is required independent of the IFN-λ response.** WT (A,
830 C) or *Ifnlr1*$^{-/-}$ (B, D) mice were infected by oral gavage with either 1e6 PFU or 1e7 PFU, as
831 indicated. Fecal samples (A, B) were collected at 3, 7, 14, and 21 days post-infection, and colon
832 tissue (C, D) was harvested at 21 days post-infection. All samples were analyzed via RT-qPCR,
833 and the mean of each group (N=4) is indicated. Dotted lines indicate limit of detection.

Figure 6

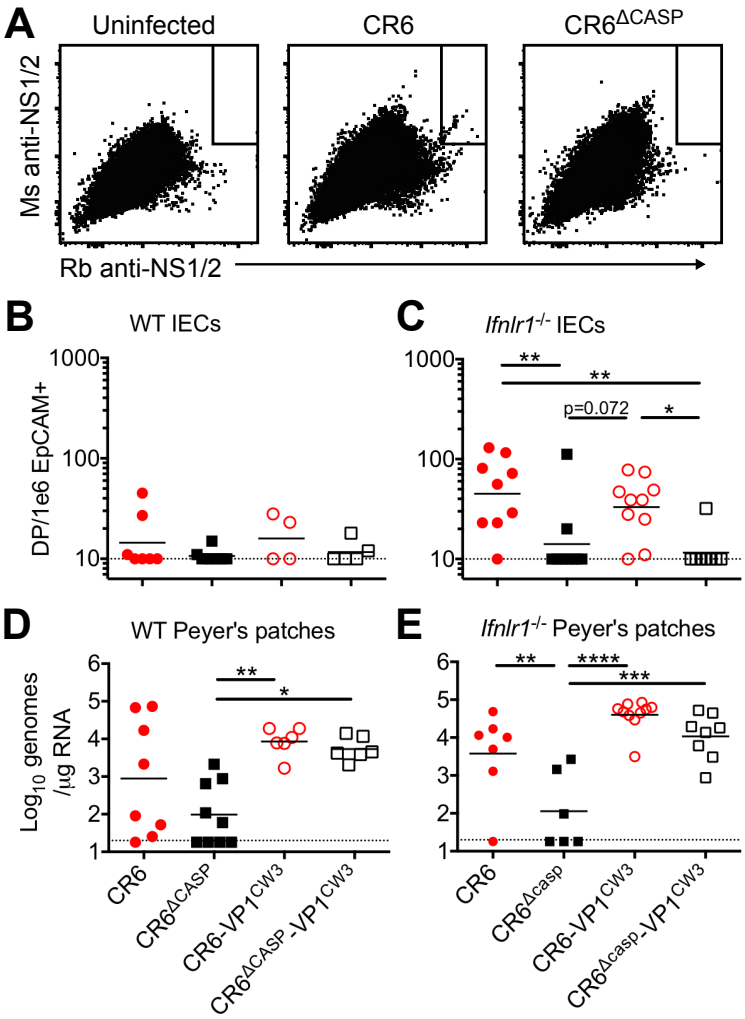

Fig. 6. NS1/2 cleavage is necessary for infection of intestinal epithelial cells. Mice deficient for the IFN-λ receptor (A, C, E) or matched receptor-sufficient controls (B, D) were infected with indicated viruses and analyzed at three days post-infection. (A-C) Intestinal epithelial cells (CD45-, EpCAM+) were collected and doubly stained for NS1/2 as described in methods. (A) Flow plots representing concatenated data from five mice in C. Dotted line indicates limit of detection. (D-E) Peyer's patches were collected and analyzed via qPCR for MNV genomic RNA and normalized to RPS29. Data are combined from at least three separate experiments. Statistical significance determined by one-way ANOVA with Tukey's multiple comparisons test. *, $p \leq 0.05$; **, $p \leq 0.01$; ***, $p \leq 0.001$; ****, $p \leq 0.0001$.

Figure 7

A

WT mice	Epithelial Infection	NON-epithelial Infection
● CR6	7/7	3/7
■ CR6$^{\Delta CASP}$	0/6	1/6
○ CR6-VP1^{CW3}	2/6	3/6
□ CR6$^{\Delta CASP}$-VP1^{CW3}	0/5	2/5

B

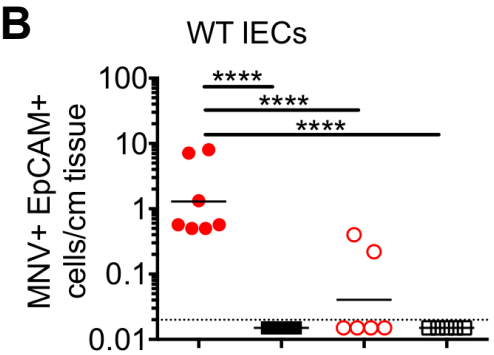

C

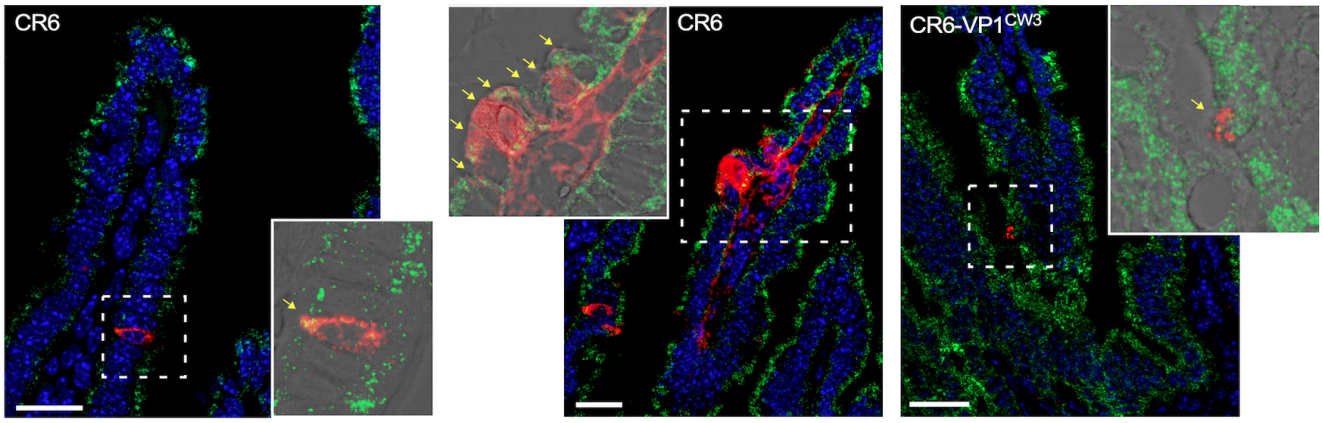

D

DKO mice	Epithelial Infection	NON-epithelial Infection
● CR6	4/4	2/4
■ CR6$^{\Delta CASP}$	0/3	0/3
○ CR6-VP1^{CW3}	7/7	7/7
□ CR6$^{\Delta CASP}$-VP1^{CW3}	0/2	2/2

E

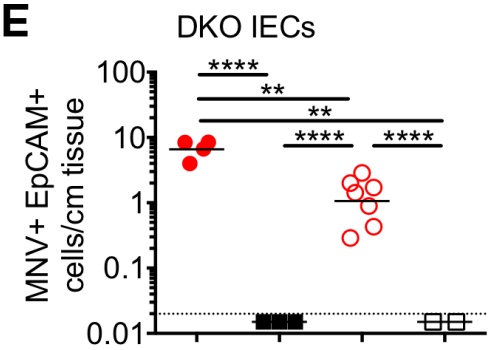

F

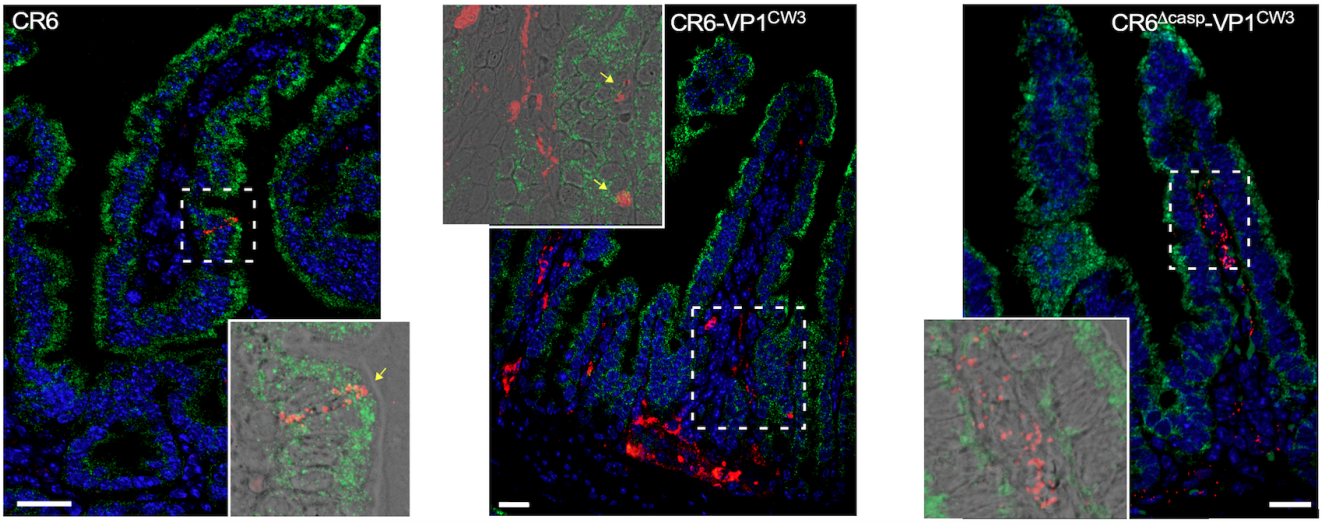

844

845 **Fig. 7. NS1/2 cleavage is necessary for infection of intestinal epithelial cells.** Ileum tissue
846 from MNV-infected WT (A-C) or DKO (D-F) mice was analyzed via RNAscope at 2-3 days post-
847 infection. MNV RNA is in red, EpCAM is in green, and nuclei are stained with DAPI in blue. The
848 tables in A and D indicate the total number of mice analyzed and the number of mice with MNV
849 genome-positive cells in epithelial (EpCAM-positive) or non-epithelial (EpCAM-negative)
850 compartments. Yellow arrows in images indicate MNV+ EpCAM+ cells. Data points in B and E
851 represent individual mice and indicate the number of MNV+ EpCAM+ cells per cm of tissue. White
852 scale bar, 20μm. Statistical significance determined by one-way ANOVA with Tukey's multiple
853 comparisons test. **, $p \leq 0.01$; ****, $p \leq 0.0001$.
854
855

Figure 8

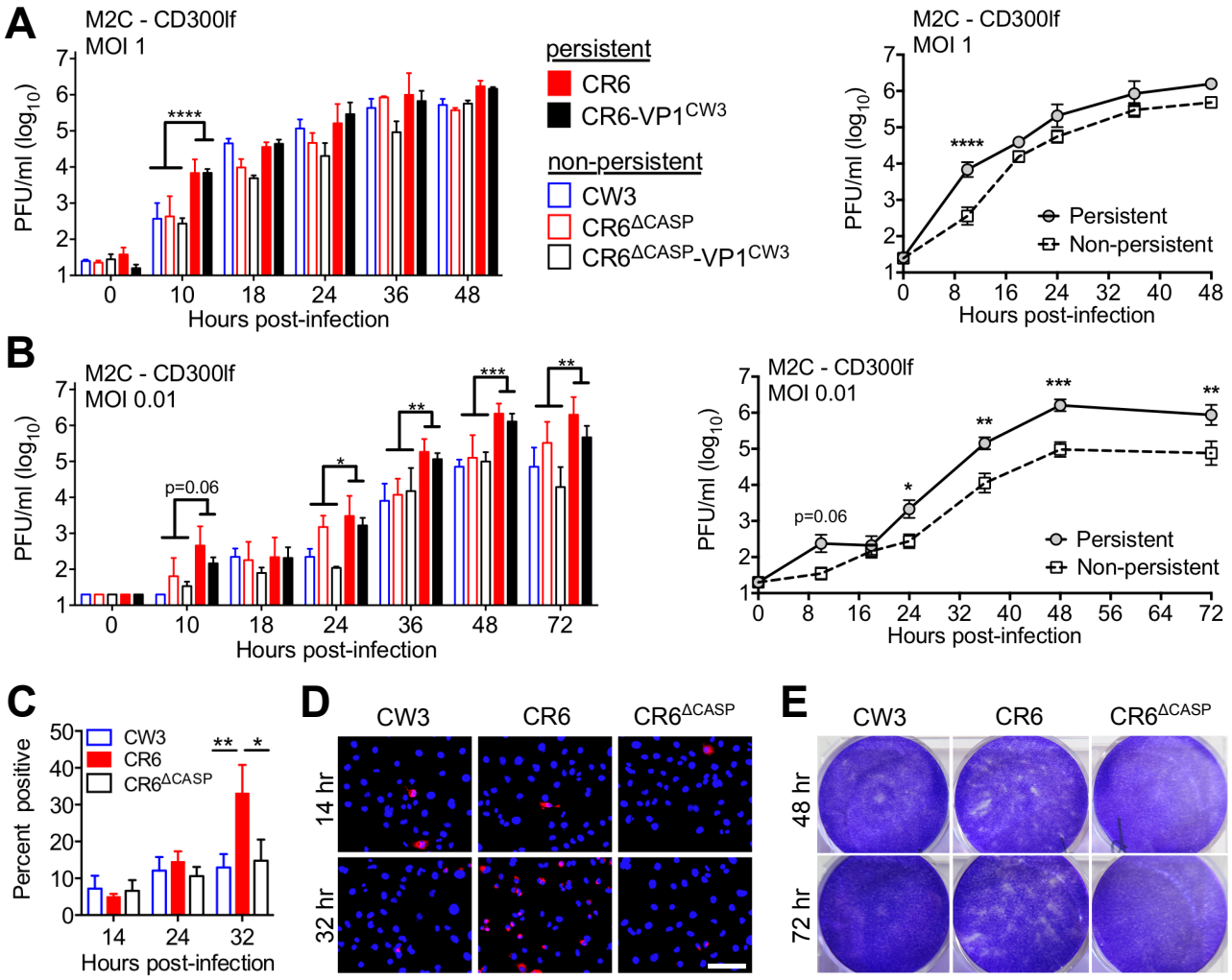

Fig. 8. NS1/2 cleavage promotes spread among IEC monolayers. (A-B) M2C-CD300lf cells were infected with the indicated strains at MOI of 1 (A) or 0.01 (B) and production of infectious MNV was monitored over time by plaque assay on BV2 cells. Curves show growth of strains grouped by persistence phenotype. (C-E) M2C-CD300lf cells were infected with the indicated strains at MOI of 1 (C-D) or 0.1 (E) and stained for MNV NS7 immunofluorescence microscopy at the indicated time post-infection (C-D) or stained with crystal violet dye to visualize the cell monolayer (E). Data in A-C is grouped from at least three independent experiments. D and E are representative images, and white scale bar is 100μm. Statistical significance determined by two-way ANOVA of grouped data with Tukey's multiple comparison test. *, $p \leq 0.05$; **, $p \leq 0.01$; ***, $p \leq 0.001$; ****, $p \leq 0.0001$.

Figure 9

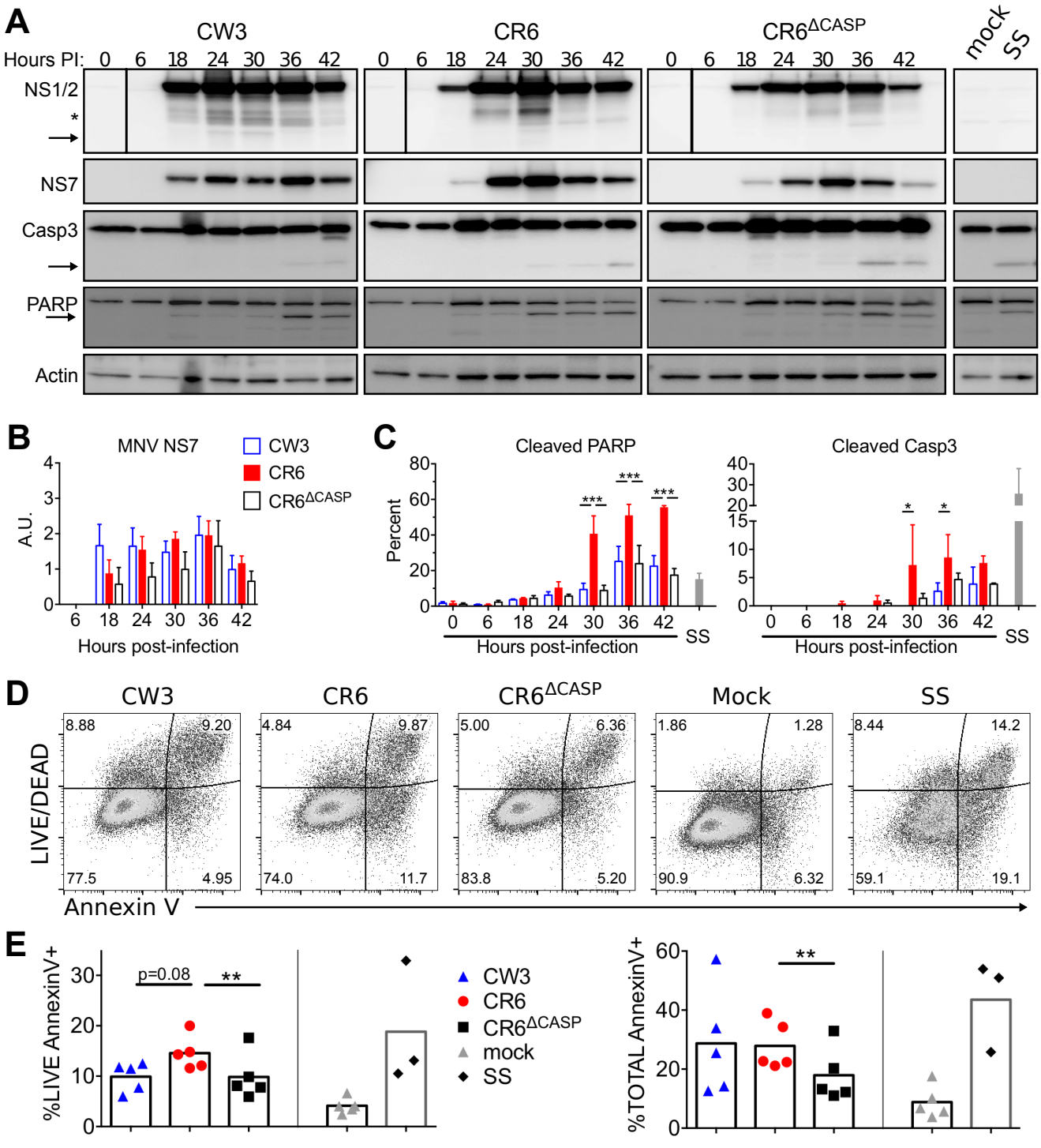

867

868 **Fig. 9. NS1/2 cleavage promotes death of IECs.** M2C-CD300lf cells were infected (MOI=1)
869 with indicated MNV strains. (A-C) Whole cell extracts were collected at indicated times and
870 analyzed via WB for MNV NS1/2, caspase 3, PARP, actin, and MNV NS7. (A) Arrows denote
871 cleaved fragments of NS1/2, caspase 3 and PARP. Images are representative of three

872 independent experiments. (B) NS7 normalized to actin analyzed via densitometry. (C) Cleaved
873 PARP and Caspase 3 were quantitated as a proportion of total protein by densitometry. (D-E)
874 Cells were harvested at 36 hours post-infection, stained with Annexin V and LIVE/DEAD viability
875 stain, and analyzed via flow cytometry. (D) Representative flow plots. (E) Live, Annexin V+, and
876 total Annexin V+ cells are graphed and mean values are indicated. Data is from three to five
877 independent experiments. Statistical significance was determined by one-way (E) or two-way (B-
878 C) ANOVA with Tukey's multiple comparison test. *, $p \leq 0.05$; **, $p \leq 0.01$; ***, $p \leq 0.001$; SS,
879 staurosporine.
880

Figure 10

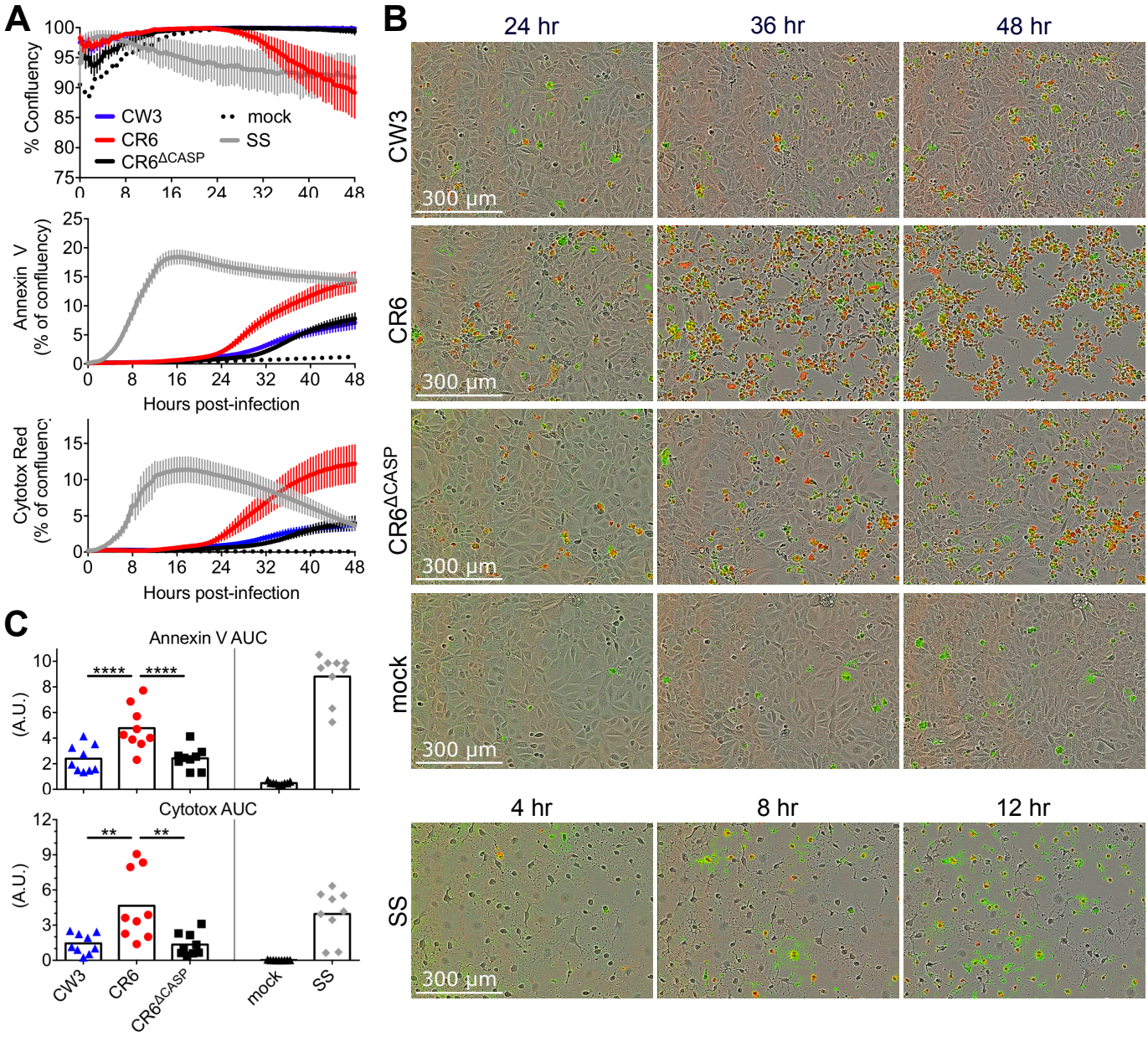

881

882 **Fig. 10. NS1/2 cleavage promotes death of IECs.** M2C-CD300lf cells were infected (MOI=1)
883 with indicated MNV strains. Cells were imaged for 48 hours on the incucyte platform in the
884 presence of Annexin V and cytotox red. (A) Quantitation of confluency, Annexin V area normalized
885 to confluency, and cytotox red area normalized to confluency over time. (B) Representative
886 images from indicated times post-infection. See also videos S1-S5. (C) Area under the curve was
887 quantitated for data in A. Data points indicate individual wells. Data in A and C is combined from
888 three independent experiments. Statistical significance in C determined by one-way ANOVA with

889 Tukey's multiple comparison test. **, p ≤ 0.01; ****, p ≤ 0.0001; AUC, area under curve; SS,
890 staurosporine.
891

Figure 11

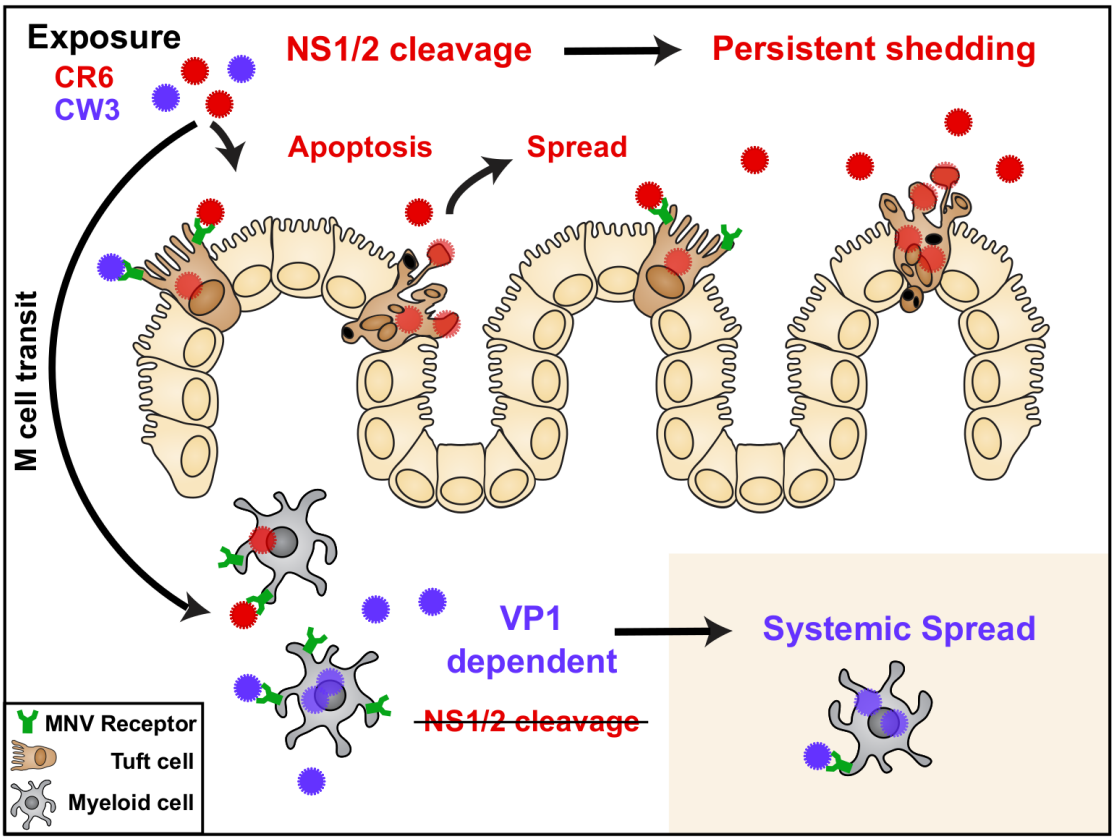

892

893 **Fig. 11. Model.** MNV can cross the epithelial barrier via M cells and replicate in myeloid cells
894 therein [24,67]. The capsid (VP1) of non-persistent strain CW3 (blue) promotes acute replication
895 in intestinal myeloid cells and is required for spread to myeloid cells of systemic tissues. A different
896 MNV gene, NS1 of persistent strain CR6 (red) is required for establishment of infection in rare
897 CD300lf-expressing IECs (tuft cells), the cellular reservoir of persistent intestinal infection and
898 fecal shedding. Cleavage of CR6 NS1 from precursor NS1/2 promotes robust tuft cell infection by
899 potentiating apoptotic caspase activity, death of infected tuft cells, and spread to dispersed target
900 cells within the intestinal epithelium. The role for NS1 and NS1/2 cleavage is specific to the
901 intestinal epithelium because NS1/2 cleavage is not required for systemic replication.

902

903 **Supporting information**

904 **S1 Video.** M2C-CD300lf cells infected with MNV strain CW3, related to figure 10.

905 **S2 Video.** M2C-CD300lf cells infected with MNV strain CR6, related to figure 10.

906 **S3 Video.** M2C-CD300lf cells infected with MNV strain CR6$^{\Delta casp}$, related to figure 10.

907 **S4 Video.** Mock-infected M2C-CD300lf cells, related to figure 10.

908 **S5 Video.** M2C-CD300lf cells treated with staurosporine, related to figure 10.